Journal of Physics and Chemistry of Solids 152 (2021) 109773

Contents lists available at ScienceDirect

Journal of Physics and Chemistry of Solids

journal homepage: http://www.elsevier.com/locate/jpcs

Effective real-space correlations of crystal lattice vibrations

Roman Tomaschitz

Sechsschimmelgasse 1/21-22, A-1090, Vienna, Austria

ARTICLE INFO

Keywords:
Effective phonon fields
Temperature-dependent permeabilities
Lattice heat capacity and Debye-Waller B-factors
Zero-point energy of lattice vibrations
Correlation functions of the copper lattice

ABSTRACT

Effective phonon fields coupled to a temperature-dependent permeability tensor are introduced to model empirical thermodynamic functions of crystal lattices and the temperature variation of Debye-Waller factors inferred by X-ray, γ-ray or neutron diffraction. The permeabilities generate a varying Debye temperature and a temperature-dependent spectral cutoff in the partition function as well as an effective temperature-dependent oscillator mass, to be calculated from diffraction and heat capacity data. The zero-point internal energy of the phonon field is extracted from low-temperature Debye-Waller *B*-factor measurements. The varying spectral cutoff, Debye temperature and oscillator mass determine the temperature evolution of real-space correlation functions. Closed integral representations are derived for the effective two-point function correlating isotropic lattice vibrations in monatomic cubic crystals as well as for the reduced four-point function correlating fluctuations around the mean-squared atomic displacement. The correlations are long-range with power-law tails and become oscillatory at low temperature. The formalism is illustrated with the correlation functions of copper.

1. Introduction

The aim is to develop an effective field theory of phonons that can accurately model empirical thermodynamic functions and Debye-Waller factors. To this end, we employ temperature-dependent permeabilities in the Lagrangian of the wave field. In the bosonic quantization resulting in the phonon partition function, the permeabilities emerge as temperature-dependent Debye temperature and spectral cutoff and give rise to a temperature-dependent effective oscillator mass. We also demonstrate that the varying Debye temperature, spectral cutoff and oscillator mass can unambiguously be reconstructed from measurements of the heat capacity and vibrational amplitudes defining the Debye-Waller *B*-factors. The field theory is first worked out for monatomic cubic lattices and subsequently extended to anisotropic compound crystals.

The crossover from the cubic low-temperature scaling of the lattice heat capacity to the constant high-temperature regime is usually not very accurately reproduced by a constant Debye temperature and spectral cutoff, so that a temperature-dependent Debye temperature $\theta(T)$ has been frequently invoked to model this crossover [1–8]. However, a phonon partition function with varying Debye temperature does not define an equilibrium system, since the equilibrium condition $\partial S/\partial U = 1/T$ on the internal-energy derivative of entropy is violated. In Ref. [9], it was demonstrated that this equilibrium condition can be preserved by allowing the spectral cutoff $\Lambda(T)$ of the partition function to also vary with temperature, in addition to $\theta(T)$. Here, we provide the underlying field-theoretic framework for a varying Debye temperature, spectral cutoff and oscillator mass; the latter does not affect the thermodynamic variables but enters in Debye-Waller factors and correlation functions.

The proposed effective field theory of lattice vibrations is non-perturbative; in particular, it does not require anharmonic modifications of the oscillator potential or the introduction of a non-uniform density of states or the addition of Einstein terms at optical frequencies. The derived phonon partition function defines a genuine equilibrium system, despite the temperature dependence of the Debye temperature. The temperature variation of $\theta(T)$ and $\Lambda(T)$ improves the accuracy of the Debye heat capacity in the intermediate temperature range where occasionally a phonon excess emerges unaccounted for by the standard theory.

X-ray, γ-ray and neutron diffraction measurements of Debye-Waller *B*-factors suggest a faster-than-linear increase of the *B*-factors at high temperature, in contrast to the prediction of the Debye theory. The constant Debye temperatures inferred from caloric and diffraction measurements usually also differ in the standard theory. Here, we show that the varying Debye temperature extracted from the experimental heat capacity is also suitable to model the temperature evolution of empirical Debye-Waller *B*-factors, which is accurately reproduced by a temperature-dependent Debye temperature and oscillator mass over the full temperature range up to the melting point. (The varying spectral cutoff of the thermodynamic variables scales out in *B*-factors.) The

E-mail address: tom@geminga.org.

https://doi.org/10.1016/j.jpcs.2020.109773
Received 19 July 2020; Received in revised form 3 September 2020; Accepted 19 September 2020
Available online 12 October 2020

attempt here is to model observables depending on Debye temperature, spectral cutoff and oscillator mass consistently with the same set of temperature-dependent functions. Another example to that effect, apart from thermodynamic functions and B-factors studied in this paper, is the electrical and thermal resistivity of metals due to electron-phonon scattering, where the Debye temperature enters in the Bloch-Grüneisen integral.

The zero-point internal energy of the phonons is extracted from the zero-temperature limit of the empirical B-factors. This is another marked difference to the Debye theory, where the zero-point energy is already determined by the constant caloric Debye temperature and usually differs from the value obtained from low-temperature B-factor diffraction measurements.

Once the temperature variation of the spectral cutoff, Debye temperature and effective oscillator mass has been reconstructed from empirical data, closed integral representations for the real-space correlation functions can be obtained. We will derive the effective two-point correlation of lattice vibrations as a function of temperature and distance, and also the four-point correlation of fluctuations around the mean-squared atomic displacement. The short- and long-distance asymptotics of these correlations, which become oscillatory at low temperature, will be discussed as well.

A specific example will be studied, the correlation functions of the copper lattice, but the method introduced here to infer the effective partition and correlation functions from heat capacity data and empirical Debye-Waller factors has much wider applicability and can be extended to anisotropic (non-cubic) and compound crystals as done in Section 6. Possible recently studied applications include Heusler and half-Heusler alloys [10–17], perovskites [18,19], intermetallics [20], zinc-blende alloys [21,22], cuprates [23], zirconates [24,25], transition-metal nitrides [26], rare-earth compounds [27,28], etc. There are no particular requirements as to the material parameters. Microscopic interactions are modeled effectively by permeability tensors, which can be reconstructed from the empirical heat capacity and Debye-Waller factors of the atomic constituents in the formula unit.

This paper is organized as follows. In Section 2.1, we introduce the effective phonon field of monatomic cubic lattices, coupled to a temperature-dependent permeability tensor. The purpose of this tensor is to effectively account for anharmonicity and deviations from the uniform density of states assumed in the Debye theory. The Lagrange formalism and quantization are outlined, and the partition function, internal energy and entropy of lattice vibrations in elemental cubic crystals are derived. (In Sections 2-5, the field theory is developed for elemental cubic crystals, and a step-by-step extension of the formalism to anisotropic compounds is given in Section 6.) In Section 2.2, the effect of temperature-dependent permeabilities on the two-point correlation function of atomic vibrational displacements is analyzed in real space, including the zero-distance limit which defines the Debye-Waller B-factor. The permeabilities in the Lagrangian can be reconstructed from the varying Debye temperature $\theta(T)$, spectral cutoff $\Lambda(T)$ and effective oscillator mass $m_{\rm eff}(T)$, whose temperature dependence is inferred from heat capacity and B-factor measurements.

In Section 3 and Appendix A, the real-space four-point autocorrelation of lattice vibrations in monatomic cubic crystals is derived. Like the two-point function, this correlation depends on $\theta(T)$, $\Lambda(T)$ and $m_{\rm eff}(T)$. The reduced four-point function correlates fluctuations around the mean-squared displacement, and the zero-distance limit of this correlation determines the next-to-leading order in the cumulant expansion of the $\exp(-2M)$ Debye-Waller intensity factor. In Appendix A, the long-range asymptotics of two- and four-point lattice correlations is studied. The correlations are nearly constant at short distance and admit long-range power-law decay; oscillations emerge at low temperature in the crossover regime, without affecting the positivity of the correlations. In contrast to other bosonic systems, the correlations are singularity free, like the zero-point lattice energy, because of the spectral cutoff.

In Section 4.1, the calculation of the temperature-dependent spectral cutoff $\Lambda(T)$ and Debye temperature $\theta(T)$ from the molar internal energy and entropy is explained; the latter are obtained from the empirical isochoric lattice heat capacity and diffraction measurements of the B-factor. In Sections 4.2, 4.3 and Appendix B, the high- and low-temperature limits of $\Lambda(T)$ and $\theta(T)$ are derived, and a relation between the zero-temperature limit of the $B(T)$-factor and the zero-point internal energy is pointed out, so that low-temperature measurements of the B-factor can be used to infer the zero-point lattice energy.

In Section 5, the real-space correlations of lattice vibrations in copper are studied. Available heat capacity data of copper [33] cover the low- and high-temperature regimes as well as the crossover where deviations from the Debye heat capacity emerge, and an accurate Mössbauer γ-ray determination of the Debye-Waller B-factor over an extended temperature range is also on hand [37]. First, a least-squares fit is performed to the empirical lattice heat capacity, using a multiply broken power-law density as fit function. Then the zero-point internal energy is extracted from the low-temperature limit of B-factor measurements, and the temperature evolution of the lattice entropy and thermal component of the internal energy is obtained by integrations of the regressed heat capacity. These empirical functions, entropy and internal energy, unambiguously determine the temperature dependence of the spectral cutoff $\Lambda(T)$ of the partition function and the varying Debye temperature $\theta(T)$ as well as the effective phonon speed $c_{\rm eff}(T)$ in the dispersion relation. The effective oscillator mass $m_{\rm eff}(T)$ is calculated from the measured temperature variation of the B-factor; $m_{\rm eff}(T)$ coincides with the atomic mass at zero temperature, but is otherwise temperature dependent. Having determined these variables, the two-point autocorrelation of lattice vibrations in copper and the reduced four-point function correlating fluctuations around the mean-squared vibrational amplitude of the copper atoms are calculated as functions of distance and temperature, and their properties are discussed.

In Section 6, we explain the extension of the field theory outlined above for monatomic cubic crystals to (anisotropic) compounds. In this case, different Debye temperatures $\theta_j(T)$ and spectral cutoffs $\Lambda_j(T)$ are employed for the field components (indexed by j), to be determined from the Debye-Waller factors $B_j(T)$ of the respective atomic constituents of the compound. In Section 7, we present our conclusions.

2. Effective phonon fields coupled to permeability tensors

2.1. Temperature-dependent permeabilities, effective partition function, internal energy and entropy of lattice vibrations

We start by modeling lattice vibrations with a massless real 3-vector field $u_n(\mathbf{x},t)$, $n=1,2,3$, coupled to an isotropic permeability tensor $g^{\alpha\beta}$ with components $g^{00}=-\mu^{1/2}\varepsilon$, $g^{ab}=\delta^{ab}/\mu^{1/2}$ and $g^{a0}=0$, where $\varepsilon(T)$ and $\mu(T)$ are positive temperature-dependent permeabilities. The Lagrangian of the field reads $L=-\sum_n g^{\alpha\beta}\partial_\alpha u_n\partial_\beta u_n/2$ or $L=\sum_n(\mu^{1/2}\varepsilon(\partial_t u_n)^2/2-(\nabla u_n)^2/(2\mu^{1/2}))$, leading to the wave equations $g^{\alpha\beta}\partial_\alpha\partial_\beta u_n=0$ or $(\Delta-\mu\varepsilon\partial_t^2)u_n=0$ for the vibrations. (Summation over Greek indices $\alpha,\beta=0,\ldots,3$ is implied.) The energy density and flux vector read

$$\rho=\sum_{n=1}^{3}\left(\frac{1}{2}\mu^{1/2}\varepsilon(\partial_t u_n)^2+\frac{(\nabla u_n)^2}{2\mu^{1/2}}\right),\quad S_k=-\sum_{n=1}^{3}\partial_l u_n\frac{\partial_k u_n}{\mu^{1/2}},\tag{2.1}$$

so that the continuity equation $\mathrm{div}\mathbf{S}+\partial_t\rho=0$ is satisfied. The wave equations are solved by the Fourier modes $\mathbf{u}^j(\mathbf{x},t;\mathbf{k})=\widehat{\boldsymbol{\varepsilon}}^j(\mathbf{k})\phi_{j,\mathbf{k}}e^{i(\mathbf{kx}-\omega_{\mathbf{k}}t)}$, with temperature-dependent frequencies defined by the dispersion relation $\omega_{\mathbf{k}}=c_{\rm eff}(T)k$, where $c_{\rm eff}=1/\sqrt{\varepsilon(T)\mu(T)}$ is the effective phonon speed (the same for longitudinal and transversal modes, being the counterpart to the averaged constant sound velocity of the Debye theory) and $\mathbf{k}=k\mathbf{k}_0$ with unit wave vector $\mathbf{k}_0$. The $\widehat{\boldsymbol{\varepsilon}}^j(\mathbf{k})$ constitute a triad of orthonormal polarization vectors, in particular $\widehat{\boldsymbol{\varepsilon}}^3(\mathbf{k})=\mathbf{k}_0$ and

$\sum_j \widehat{\varepsilon}^j_m(\mathbf{k})\widehat{\varepsilon}^j_n(\mathbf{k}) = \delta_{mn}$. (Upper indices refer to the polarization triad and lower ones to vector components.)

We will use box quantization, discretizing the wave vector as $\mathbf{k} = 2\pi\mathbf{n}/L$, $\mathbf{n} \in Z^3$, where L is the box size. The Fourier decomposition of the polarization components of the wave field $u_n = \sum_j u^j_n$ reads

$$u^j_n(\mathbf{x},t) = \frac{1}{\sqrt{2L^3}}\sum_{\mathbf{k}} \widehat{\varepsilon}^j_n(\mathbf{k})\left(\phi_{j,k}\mathrm{e}^{\mathrm{i}(\mathbf{kx}-\omega_{\mathbf{k}}t)} + \phi^*_{j,\mathbf{k}}\mathrm{e}^{-\mathrm{i}(\mathbf{kx}-\omega_{\mathbf{k}}t)}\right), \tag{2.2}$$

with expansion coefficients $\phi_{j,\mathbf{k}}$. The time-averaged products

$$\begin{aligned}
&\sum_n \partial_t u^i_n \partial_t u^l_n = L^{-3}\delta^{jl}\sum_k \omega^2_{\mathbf{k}}\phi_{j,\mathbf{k}}\phi^*_{j,\mathbf{k}},\\
&\sum_n \nabla u^i_n\cdot\nabla u^l_n = L^{-3}\delta^{jl}\sum_k k^2\phi_{j,\mathbf{k}}\phi^*_{j,\mathbf{k}},\\
&\sum_n \partial_t u^i_n \nabla u^l_n = -L^{-3}\delta^{jl}\sum_{\mathbf{k}} \mathbf{k}\omega_{\mathbf{k}}\phi_{j,\mathbf{k}}\phi^*_{j,\mathbf{k}},
\end{aligned} \tag{2.3}$$

are needed to obtain the mode decomposition of the time-averaged energy density and flux vector, summed over the polarization components,

$$\rho(\mathbf{x}) = \frac{1}{L^3}\sum_{j,\mathbf{k}} \mu^{1/2}\varepsilon\omega^2_{\mathbf{k}}\phi_{j,\mathbf{k}}\phi^*_{j,\mathbf{k}} = \frac{1}{2}\frac{1}{L^3}\sum_{j,\mathbf{k}}\omega_{\mathbf{k}}\left(a^\dagger_{j,\mathbf{k}}a_{j,\mathbf{k}} + a_{j,\mathbf{k}}a^\dagger_{j,\mathbf{k}}\right), \tag{2.4}$$

$$\mathbf{S}(\mathbf{x}) = \frac{1}{L^3}\sum_{j,\mathbf{k}} \mathbf{k}_0\varepsilon^{1/2}\omega^2_{\mathbf{k}}\phi_{j,\mathbf{k}}\phi^*_{j,\mathbf{k}} = \frac{1}{2}\frac{1}{L^3}\sum_{j,\mathbf{k}}\mathbf{k}_0\frac{\omega_{\mathbf{k}}}{\sqrt{\varepsilon\mu}}\left(a^\dagger_{j,\mathbf{k}}a_{j,\mathbf{k}} + a_{j,\mathbf{k}}a^\dagger_{j,\mathbf{k}}\right). \tag{2.5}$$

Here, we replaced the field amplitudes by bosonic annihilation and creation operators $\phi_{j,\mathbf{k}}\to a_{j,\mathbf{k}}/\sqrt{\mu^{1/2}\varepsilon\omega_{\mathbf{k}}}$, $\phi^*_{j,\mathbf{k}}\to a^\dagger_{j,\mathbf{k}}/\sqrt{\mu^{1/2}\varepsilon\omega_{\mathbf{k}}}$, and symmetrized. The normalization is chosen so that the effective Hamiltonian admits the temperature-dependent harmonic oscillator representation $H_{\mathrm{eff}} = \int_{L^3}\rho(\mathbf{x},t)\mathrm{d}\mathbf{x} = \sum_{j,\mathbf{k}}\omega_{\mathbf{k}}(T)(N_{j,\mathbf{k}} + 1/2)$, where the $N_{j,\mathbf{k}} = a^\dagger_{j,\mathbf{k}}a_{j,\mathbf{k}}$ are commuting hermitian particle number operators, and we used the commutation relations $[a_{j,\mathbf{k}}, a^\dagger_{l,\mathbf{k}'}] = \delta_{\mathbf{k}\mathbf{k}'}\delta_{jl}$. The quantized energy density (2.4) reads $\rho = H_{\mathrm{eff}}/L^3$. A multi-index notation $i = (j,\mathbf{k})$ will be employed as shortcut for the summation indices. The a_i and their adjoints satisfy the commutation relations $[a_i, a^\dagger_n] = \delta_{in}$, $[a_i, a_n] = 0$, $[a^\dagger_i, a^\dagger_n] = 0$, as well as $[a_n, N_m] = \delta_{nm}a_n$ and $[a^\dagger_n, N_m] = -\delta_{nm}a^\dagger_n$.

The statistical operator reads $\widehat{\rho} = \exp(-H_{\mathrm{eff}}(T)/T)$, the partition function is defined by the trace $Z = \mathrm{Tr}[\widehat{\rho}]$, and the total internal energy is obtained as expectation value $U = \langle H_{\mathrm{eff}}\rangle_T = \mathrm{Tr}[H_{\mathrm{eff}}\widehat{\rho}]/Z$. The expectation value of an operator of type $G_j = \sum_{\mathbf{k}} g_{j,\mathbf{k}}(N_{j,\mathbf{k}} + 1/2)$ reads, in bosonic quantization at finite temperature [29],

$$\left\langle G_j\right\rangle_T = \frac{L^3}{(2\pi)^3}\int g_{j,\mathbf{k}}\left(\frac{1}{\mathrm{e}^{\omega_{\mathbf{k}}/T}-1} + \frac{1}{2}\right)\mathrm{d}\mathbf{k}\,, \tag{2.6}$$

where $g_{j,\mathbf{k}}$ is an arbitrary function of j and $\mathbf{k}$ and other parameters such as temperature, atomic density and space coordinates. Applying (2.6) to the effective Hamiltonian by identifying $g_{j,\mathbf{k}} = \omega_{\mathbf{k}}(T)$, we find the total internal energy $U = \sum_j\langle H_{\mathrm{eff},j}\rangle_T$, with polarization components

$$\left\langle H_{\mathrm{eff},j}\right\rangle_T = \frac{4\pi L^3}{(2\pi)^3}\int_0^{\Lambda(T)} \omega_{\mathbf{k}}(T)\left(\frac{1}{\mathrm{e}^{\omega_{\mathbf{k}}(T)/T}-1} + \frac{1}{2}\right)k^2\mathrm{d}k, \tag{2.7}$$

where $\omega_{\mathbf{k}} = c_{\mathrm{eff}}(T)k$ and $c_{\mathrm{eff}} = 1/\sqrt{\varepsilon(T)\mu(T)}$. The upper integration boundary in (2.7) is a temperature-dependent spectral cutoff $\Lambda(T)$ to be specified. The internal energy of the Debye theory is recovered by assuming a temperature-independent c_{eff} and Λ, cf. Section 5. Using a dimensionless integration variable, $z = \omega_{\mathbf{k}}/T$, we find the polarization components of the energy density as

$$\widehat{u}_j = \frac{\langle H_{\mathrm{eff},j}\rangle_T}{L^3} = \frac{4\pi}{(2\pi)^3}\Lambda^3 k_{\mathrm{B}}T\left(D(d) + \frac{d}{8}\right), \quad D(d) := \frac{1}{d^3}\int_0^d \frac{z^3\mathrm{d}z}{\mathrm{e}^z - 1}, \tag{2.8}$$

with $d(T) = \theta(T)/T$ and Debye temperature $\theta(T) = c_{\mathrm{eff}}(T)\Lambda(T)$, so that the internal energy density summed over the three polarizations is $\widehat{u} = U/V = \sum_j \widehat{u}_j$. The effective oscillator density is $n_{\mathrm{oscil}} = (4\pi/(2\pi)^3)\Lambda^3$. The units $\hbar = k_{\mathrm{B}} = 1$ have been restored in (2.8); we will use $1/\mathrm{cm}$ units for the spectral cutoff $\Lambda(T)$ and wavenumber k (integration variable in (2.7)), so that $\theta(T)[\mathrm{K}] = \hbar c_{\mathrm{eff}}\Lambda/k_{\mathrm{B}}$, with $c_{\mathrm{eff}}[\mathrm{cm}/\mathrm{s}]$.

The partition function $Z = \mathrm{Tr}[\widehat{\rho}]$ evaluated in occupation number representation reads, in the thermodynamic limit [9],

$$\log Z = -\frac{4\pi L^3}{(2\pi)^3}\sum_j \int_0^{\Lambda(T)}\left(\log\left(1-\mathrm{e}^{-\omega_{\mathbf{k}}(T)/T}\right) + \frac{1}{2}\frac{\omega_{\mathbf{k}}(T)}{T}\right)k^2\mathrm{d}k. \tag{2.9}$$

The entropy, $S = -\mathrm{Tr}[\widehat{\rho}_S\log\widehat{\rho}_S]$, is defined by the normalized statistical operator $\widehat{\rho}_S = \widehat{\rho}/Z$, cf. after (2.5), so that $\mathrm{Tr}[\widehat{\rho}_S] = 1$ and $S = \log Z + U/T$. Thus, by substituting (2.7) and (2.9), we find $S = \sum_j\langle S_j\rangle_T$, where

$$\langle S_j\rangle_T = \frac{4\pi L^3}{(2\pi)^3}\int_0^{\Lambda(T)}\left(\frac{\omega_{\mathbf{k}}}{T}\frac{1}{\mathrm{e}^{\omega_{\mathbf{k}}/T}-1} - \log\left(1-\mathrm{e}^{-\omega_{\mathbf{k}}/T}\right)\right)k^2\mathrm{d}k, \tag{2.10}$$

with dispersion relation $\omega_{\mathbf{k}} = c_{\mathrm{eff}}(T)k$. Integration (by parts) analogous to (2.8) gives the entropy density

$$\widehat{s}_j = \frac{\langle S_j\rangle_T}{L^3} = \frac{4\pi}{(2\pi)^3}k_{\mathrm{B}}\Lambda^3\left(\frac{4}{3}D(d) - \frac{1}{3}\log\left(1-\mathrm{e}^{-d}\right)\right), \tag{2.11}$$

with $d = \theta(T)/T$ and $\theta = c_{\mathrm{eff}}(T)\Lambda(T)$. The total entropy density of lattice vibrations is obtained by summation over the polarizations, $\widehat{s} = S/V = \sum_j \widehat{s}_j$.

2.2. Effective two-point correlations of lattice vibrations and mean-squared atomic displacement

Employing the mode decomposition (2.2) of the phonon field, we consider the product

$$\begin{aligned}
u^j_n(\mathbf{x},t)u^l_m(\mathbf{y},t) = \frac{1}{2L^3}\sum_{\mathbf{k},\mathbf{k}'}&\widehat{\varepsilon}^j_n(\mathbf{k})\widehat{\varepsilon}^l_m(\mathbf{k}')\frac{1}{\sqrt{\mu^{1/2}\varepsilon\omega_{\mathbf{k}}}}\frac{1}{\sqrt{\mu^{1/2}\varepsilon\omega_{\mathbf{k}'}}}\\
&\times\left(a^\dagger_{j,\mathbf{k}}a_{l,\mathbf{k}'}\mathrm{e}^{-\mathrm{i}(\mathbf{kx}-\omega_{\mathbf{k}}t)}\mathrm{e}^{\mathrm{i}(\mathbf{k}'\mathbf{y}-\omega_{\mathbf{k}'}t)}\right.\\
&\left.+\, a_{j,\mathbf{k}}a^\dagger_{l,\mathbf{k}'}\mathrm{e}^{\mathrm{i}(\mathbf{kx}-\omega_{\mathbf{k}}t)}\mathrm{e}^{-\mathrm{i}(\mathbf{k}'\mathbf{y}-\omega_{\mathbf{k}'}t)}\right),
\end{aligned} \tag{2.12}$$

where the upper and lower indices on u^j_n and $\widehat{\varepsilon}^j_n$ label polarization and vector components, respectively. Using the commutation relations stated after (2.5), this can be written as

$$u^j_n(\mathbf{x})u^l_m(\mathbf{y}) = \frac{\delta^{jl}}{2L^3}\sum_{\mathbf{k}}\frac{\widehat{\varepsilon}^j_n(\mathbf{k})\widehat{\varepsilon}^j_m(\mathbf{k})}{\mu^{1/2}\varepsilon\omega_{\mathbf{k}}}\left(N_{j,\mathbf{k}} + \frac{1}{2}\right)\left(\mathrm{e}^{\mathrm{i}\mathbf{k}(\mathbf{x}-\mathbf{y})} + \mathrm{e}^{-\mathrm{i}\mathbf{k}(\mathbf{x}-\mathbf{y})}\right), \tag{2.13}$$

provided that this product is employed for the calculation of expectation values, where the off-diagonal terms $\mathbf{k}\neq\mathbf{k}'$, $j\neq l$ drop out, which can easily be seen in occupation number representation [29]. (For the same reason, we omitted the $a_{j,\mathbf{k}}a_{l,\mathbf{k}'}$ and $a^\dagger_{j,\mathbf{k}}a^\dagger_{l,\mathbf{k}'}$ terms in (2.12).) The $N_{j,\mathbf{k}} = a^\dagger_{j,\mathbf{k}}a_{j,\mathbf{k}}$ denote particle number operators, cf. after (2.5). The time variable in $u^j_n(\mathbf{x},t)$ has been dropped, as the equal-time correlations are time independent.

Applying relation (2.6) for expectation values at finite temperature to the operator product (2.13), we obtain

$$\langle u_n^j(\mathbf{x})u_m^l(\mathbf{y})\rangle_T = \frac{\delta^{jl}}{2(2\pi)^3}\int_0^{\Lambda(T)}\int_{S_2}\widehat{\varepsilon}_n^j(\mathbf{k})\widehat{\varepsilon}_m^j(\mathbf{k})\frac{\mathrm{e}^{\mathrm{i}\mathbf{k}(\mathbf{x}-\mathbf{y})}+\mathrm{c.c.}}{\mu^{1/2}\varepsilon\omega_{\mathbf{k}}} \times\left(\frac{1}{\mathrm{e}^{\omega_{\mathbf{k}}/T}-1}+\frac{1}{2}\right)k^2\mathrm{d}k\mathrm{d}\Omega_{\mathbf{k}_0}, \tag{2.14}$$

where $\mathrm{d}\Omega_{\mathbf{k}_0}=\sin\theta\mathrm{d}\theta\mathrm{d}\phi$ is the solid-angle element and $\omega_{\mathbf{k}} = c_{\mathrm{eff}}(T)k$, $c_{\mathrm{eff}} = 1/\sqrt{\varepsilon(T)\mu(T)}$, see the beginning of Section 2.1. $\Lambda(T)$ is a temperature-dependent spectral cutoff, the same as in the thermodynamic functions (2.7) and (2.9). Summation over the polarizations and subsequent integration over the solid angle by way of $\int_{S_2}\mathrm{e}^{\pm\mathrm{i}\mathbf{k}\mathbf{x}}\mathrm{d}\Omega_{\mathbf{k}_0} = 4\pi\sin(kr)/(kr)$ gives

$$\langle u_n(\mathbf{x})u_m(\mathbf{y})\rangle_T = \frac{4\pi\delta_{nm}}{(2\pi)^3}\int_0^{\Lambda(T)}\frac{1}{\mu^{1/2}\varepsilon\omega_{\mathbf{k}}}\frac{\sin(kr)}{kr}\left(\frac{1}{\mathrm{e}^{\omega_{\mathbf{k}}/T}-1}+\frac{1}{2}\right)k^2\mathrm{d}k, \tag{2.15}$$

where $u_n=\sum_j u_n^j$ and $r = |\mathbf{x}-\mathbf{y}|$. Using a dimensionless integration variable z as in (2.8), we find

$$\langle u_n(\mathbf{x})u_n(\mathbf{y})\rangle_T = \frac{4\pi}{(2\pi)^3}\frac{\Lambda^3T}{\theta^2}\frac{1}{\mu^{1/2}\varepsilon}\frac{1}{d}\int_0^d\frac{\sin\left(zrT/c_{\mathrm{eff}}\right)}{zrT/c_{\mathrm{eff}}}\left(\frac{1}{\mathrm{e}^z-1}+\frac{1}{2}\right)z\mathrm{d}z, \tag{2.16}$$

where $\theta(T) = c_{\mathrm{eff}}(T)\Lambda(T)$ is the Debye temperature and $d = \theta(T)/T$. The long-range asymptotics of the two-point correlation function $C^{(2)}(r,T)=\langle u_n(\mathbf{x})u_n(\mathbf{y})\rangle_T$ in (2.16) will be studied in Appendix A. Due to the isotropic permeability tensor, $C^{(2)}(r,T)$ does not depend on the chosen vector component (labeled n).

In the short-distance limit $r = |\mathbf{x}-\mathbf{y}|\to 0$, the first ratio in the integrand of (2.16) drops out, so that the expectation value of the squared field component $\langle u_n^2(0)\rangle_T = \langle u_n(\mathbf{x})u_n(\mathbf{x})\rangle_T$ reads

$$\langle u_n^2(0)\rangle_T = \frac{4\pi}{(2\pi)^3}\frac{\Lambda^3T}{\theta^2}\frac{1}{\mu^{1/2}\varepsilon}\left(D_1(d)+\frac{d}{4}\right),$$
$$D_1(d) := \frac{1}{d}\int_0^d\frac{z\mathrm{d}z}{\mathrm{e}^z-1}. \tag{2.17}$$

In addition to the varying Debye temperature $\theta(T) = Td(T)$, spectral cutoff $\Lambda(T)$ and phonon speed $c_{\mathrm{eff}}(T) = \theta(T)/\Lambda(T)$, we introduce a temperature-dependent effective oscillator mass $m_{\mathrm{eff}}(T)$ and identify the product of the permeabilities in (2.17) as

$$\mu^{1/2}\varepsilon = \frac{4\pi}{3(2\pi)^3}m_{\mathrm{eff}}\Lambda^3 = \frac{1}{3}m_{\mathrm{eff}}(T)n_{\mathrm{oscil}}(T), \tag{2.18}$$

where $n_{\mathrm{oscil}} = (4\pi/(2\pi)^3)\Lambda^3$ is the effective oscillator density, cf. after (2.8). This choice of $\mu^{1/2}\varepsilon$ (which amounts to a normalization of the phonon field, cf. (2.2) and after (2.5)) allows us to identify the expectation value of the squared field amplitude $\langle u_n^2(0)\rangle_T$ in (2.17) with the mean-squared atomic vibration [9],

$$\langle u_n^2(0)\rangle_T = \frac{3}{m_{\mathrm{eff}}(T)}\frac{\hbar^2T}{k_{\mathrm{B}}\theta^2(T)}\left(D_1(d(T))+\frac{d(T)}{4}\right), \tag{2.19}$$

where the units ($\hbar = k_{\mathrm{B}} = 1$) have been restored, so that $\langle u_n^2(0)\rangle_T[\mathrm{cm}^2]$. The effective phonon speed is related to the permeabilities by $c_{\mathrm{eff}} = 1/\sqrt{\varepsilon(T)\mu(T)}$, cf. the beginning of Section 2.1. Combining this with $\mu^{1/2}\varepsilon = m_{\mathrm{eff}}n_{\mathrm{oscil}}/3$ in (2.18), we find the permeabilities as $\varepsilon = (c_{\mathrm{eff}}m_{\mathrm{eff}}n_{\mathrm{oscil}}/3)^2$ and $\mu = 1/(c_{\mathrm{eff}}^2m_{\mathrm{eff}}n_{\mathrm{oscil}}/3)^2$.

The final expression for the correlation function (2.16) is

$$\left\langle u_n(\mathbf{x})u_m(\mathbf{y})\right\rangle_T = \frac{3\delta_{nm}}{m_{\mathrm{eff}}}\frac{\hbar^2T^2}{k_{\mathrm{B}}\theta^3}\int_0^{\theta/T}\frac{\sin\left(zrk_{\mathrm{B}}T/(\hbar c_{\mathrm{eff}})\right)}{zrk_{\mathrm{B}}T/(\hbar c_{\mathrm{eff}})}\left(\frac{1}{\mathrm{e}^z-1}+\frac{1}{2}\right)z\mathrm{d}z, \tag{2.20}$$

with temperature-dependent Debye temperature $\theta = c_{\mathrm{eff}}(T)\Lambda(T)$, phonon speed $c_{\mathrm{eff}}(T)$, spectral cutoff $\Lambda(T)$ and oscillator mass $m_{\mathrm{eff}}(T)$. The units have been restored in (2.20).

3. Real-space four-point correlation and second-order Debye-Waller factor of elemental cubic crystals

Because of the isotropy of the permeability tensor reflecting the cubic lattice symmetry, the autocorrelation $\langle u_n(\mathbf{x})u_n(\mathbf{y})\rangle_T$ in (2.15) of the vector component $u_n(\mathbf{x})$ is identical to that of a scalar field. That is, we can treat the field components u_n in the Lagrangian, energy density and flux vector, cf. (2.1), as three scalar fields coupled to the same permeability tensor, and replace the Fourier expansion (2.2) by

$$u_n(\mathbf{x},t) = \frac{1}{\sqrt{2L^3}}\sum_{\mathbf{k}}\left(\phi_{n,\mathbf{k}}\mathrm{e}^{\mathrm{i}(\mathbf{k}\mathbf{x}-\omega_{\mathbf{k}}t)}+\phi_{n,\mathbf{k}}^*\mathrm{e}^{-\mathrm{i}(\mathbf{k}\mathbf{x}-\omega_{\mathbf{k}}t)}\right). \tag{3.1}$$

The quantization $\phi_{n,\mathbf{k}}\to a_{n,\mathbf{k}}/\sqrt{\mu^{1/2}\varepsilon\omega_{\mathbf{k}}}$, $\phi_{n,\mathbf{k}}^*\to a_{n,\mathbf{k}}^\dagger/\sqrt{\mu^{1/2}\varepsilon\omega_{\mathbf{k}}}$. of the scalar triplet (3.1) also leads to the time-averaged energy density (2.4) and flux vector (2.5). The commutation relations stated after (2.5) apply, e.g., $[a_{j,\mathbf{k}}, a_{l,\mathbf{k}'}^\dagger] = \delta_{\mathbf{k}\mathbf{k}'}\delta_{jl}$, where the indices j and l refer to the components of the scalar field triplet u_n rather than to polarization components. (Summations like $U=\sum_j\langle H_{\mathrm{eff},j}\rangle_T$ in (2.7) then also refer to the components of the triplet.) By using the scalar Fourier expansion (3.1) as starting point, we can obtain the thermodynamic variables in Section (2.1) as well as correlation functions such as (2.20) and the four-point correlation discussed below without invoking clumsy polarization triads. That is, instead of vector fields, we will use multi-component scalar fields. In the case of elemental cubic crystals, the components of the scalar triplet (3.1) are coupled to the same permeability tensor, cf. the beginning of Section 2.1. In Section 6, we will use multi-component scalar fields to effectively model compound crystals, describing (anisotropic) vibrations of the various atomic constituents by coupling the field components to different permeability tensors.

In Appendix A, we derive a closed analytic expression for the reduced equal-time four-point function of the individual field components (3.1),

$$\begin{aligned}C^{(4)}(\mathbf{x},\mathbf{y};T) &= \langle\left(u_n^2(\mathbf{x})-\langle u_n^2(0)\rangle_T\right)\left(u_n^2(\mathbf{y})-\langle u_n^2(0)\rangle_T\right)\rangle_T\\ &= \langle u_n^2(\mathbf{x})u_n^2(\mathbf{y})\rangle_T-\langle u_n^2(0)\rangle_T^2,\end{aligned} \tag{3.2}$$

which is independent of the field index n owing to isotropy. The expectation value $\langle u_n^2(0)\rangle_T$ has already been obtained in (2.17). The calculation of correlation $C^{(4)}(\mathbf{x},\mathbf{y};T)$ is sketched in Appendix A. We find

$$C^{(4)}(r,T) = C^{(4)}(\mathbf{x},\mathbf{y};T) = \langle\widehat{A}(r)\rangle_T^2+\langle\widehat{B}(r)\rangle_T\langle\widehat{A}(r)\rangle_T, \tag{3.3}$$

where

$$\left\langle\widehat{A}(r)\right\rangle_T = \frac{4\pi}{(2\pi)^3}\int_0^{\Lambda(T)}\frac{1}{\mu^{1/2}\varepsilon\omega_{\mathbf{k}}}\frac{\sin(kr)}{kr}\frac{k^2\mathrm{d}k}{\mathrm{e}^{\omega_{\mathbf{k}}/T}-1}, \tag{3.4}$$

$$\left\langle\widehat{B}(r)\right\rangle_T = \frac{4\pi}{(2\pi)^3}\int_0^{\Lambda(T)}\frac{1}{\mu^{1/2}\varepsilon\omega_{\mathbf{k}}}\frac{\sin(kr)}{kr}k^2\mathrm{d}k = \frac{4\pi}{(2\pi)^3}\frac{1}{\mu^{1/2}\varepsilon c_{\mathrm{eff}}}\frac{1}{r^2}(1-\cos(\Lambda r)), \tag{3.5}$$

with $r = |\mathbf{x}-\mathbf{y}|$, $\omega_{\mathbf{k}} = c_{\mathrm{eff}}(T)k$ and $\mu^{1/2}\varepsilon$ as in (2.18). For comparison, the two-point correlation (2.16) reads, in this notation,

$$C^{(2)}(r,T)=\langle u_n(\mathbf{x})u_n(\mathbf{y})\rangle_T=\langle\widehat{A}(r)\rangle_T+\frac{1}{2}\langle\widehat{B}(r)\rangle_T\,, \tag{3.6}$$

which is already reduced, since $\langle u_n(\mathbf{x})\rangle_T=0$. We also record the identities

$$\left\langle u_n^2(0)\right\rangle_T=\left\langle\widehat{A}(0)\right\rangle_T+\frac{1}{2}\left\langle\widehat{B}(0)\right\rangle_T, \tag{3.7}$$

$$\left\langle u_n^2(\mathbf{x})u_n^2(\mathbf{y})\right\rangle_T=\left\langle\widehat{A}(r)\right\rangle_T^2+\left\langle\widehat{B}(r)\right\rangle_T\left\langle\widehat{A}(r)\right\rangle_T+\left\langle u_n^2(0)\right\rangle_T^2, \tag{3.8}$$

$$\left\langle u_n^4(0)\right\rangle_T=2\left\langle\widehat{A}(0)\right\rangle_T^2+2\left\langle\widehat{B}(0)\right\rangle_T\left\langle\widehat{A}(0)\right\rangle_T+\frac{1}{4}\left\langle\widehat{B}(0)\right\rangle_T^2, \tag{3.9}$$

and the cumulant $\widehat{\kappa}_T:=3\langle u_n^2(0)\rangle_T^2-\langle u_n^4(0)\rangle_T$, cf. (3.15),

$$\widehat{\kappa}_T=\left\langle\widehat{A}(0)\right\rangle_T^2+\left\langle\widehat{B}(0)\right\rangle_T\left\langle\widehat{A}(0)\right\rangle_T+\frac{1}{2}\left\langle\widehat{B}(0)\right\rangle_T^2. \tag{3.10}$$

Finally we substitute $c_{\rm eff}(T)=\theta(T)/\Lambda(T)$, cf. after (2.8), and $\mu^{1/2}\varepsilon=4\pi m_{\rm eff}(T)\Lambda^3(T)/(3(2\pi)^3)$, cf. (2.18), into $\langle\widehat{A}(r)\rangle_T$ and $\langle\widehat{B}(r)\rangle_T$ as stated in (3.4) and (3.5), and restore the units to find

$$\left\langle\widehat{A}(r)\right\rangle_T=\frac{3}{m_{\rm eff}}\frac{\hbar^2T^2}{k_{\rm B}\theta^3}\int_0^{\theta/T}\frac{\sin(zT\Lambda r/\theta)}{zT\Lambda r/\theta}\frac{z\mathrm{d}z}{\mathrm{e}^z-1},\left\langle\widehat{A}(0)\right\rangle_T=\frac{3}{m_{\rm eff}}\frac{\hbar^2T}{k_{\rm B}\theta^2}D_1(\theta/T), \tag{3.11}$$

where $D_1(d)$ denotes the Debye function in (2.17), and

$$\left\langle\widehat{B}(r)\right\rangle_T=\frac{3}{m_{\rm eff}}\frac{\hbar^2}{k_{\rm B}\theta}\frac{1}{\Lambda^2r^2}(1-\cos(\Lambda r)),\quad\left\langle\widehat{B}(0)\right\rangle_T=\frac{3}{2m_{\rm eff}}\frac{\hbar^2}{k_{\rm B}\theta}\,. \tag{3.12}$$

The spectral cutoff $\Lambda(T)$ and wavenumber k are in 1/cm units, cf. (3.4) and (3.5), and $\theta(T)=\hbar c_{\rm eff}(T)\Lambda(T)/k_{\rm B}$, with $c_{\rm eff}$[cm/s], cf. the beginning of Section 2.1. The units of $\langle\widehat{A}(r)\rangle_T$ and $\langle\widehat{B}(r)\rangle_T$ are cm^2, and atomic mass units will be used for the effective oscillator mass $m_{\rm eff}(T)$.

At zero temperature, $\langle\widehat{A}(r)\rangle_{T=0}=0$, since the r dependent ratio of the integrand in (3.11) drops out, so that one can invoke $D_1(d\to\infty)\sim\pi^2/(6d)$ and use the fact that $\theta(T=0)$ stays finite, cf. Section 4.3. The average $\langle\widehat{B}(r)\rangle_T$ in (3.12) and the two-point correlation $C^{(2)}(r,T)$ in (3.6) remain finite at $T=0$, since $\theta(T=0)$, $\Lambda(T=0)$ and $m_{\rm eff}(T=0)$ are finite. The reduced four-point function $C^{(4)}(r,T)$ in (3.3) vanishes at $T=0$, since $\langle\widehat{A}(r)\rangle_{T=0}=0$.

The relative fluctuations $\sigma/\langle u_n^2(0)\rangle_T$, $\sigma=\sqrt{\langle u_n^4(0)\rangle_T-\langle u_n^2(0)\rangle_T^2}$, of the mean-squared vibrational amplitude can also be assembled from (3.7)-(3.12). The fluctuations vanish at low temperature, $\sigma/\langle u_n^2(0)\rangle_T\sim 2\pi T/\left(\sqrt{3}\,\theta(T)\right)$. In the high-temperature limit (which is not attained below the melting point), $\sigma/\langle u_n^2(0)\rangle_T\sim 1$, where we used $D_1(d\to0)\sim1$ in (3.11).

In Section 5, we will study the Debye-Waller intensity attenuation factor $\exp(-2M)$, which can be expanded as, cf. Ref. [31],

$$M\left(Q^2,T\right)=\frac{Q^2}{(4\pi)^2}\left(B(T)+B_2(T)Q^2+\cdots\right), \tag{3.13}$$

where $Q^2=(4\pi\sin\theta/\lambda)^2$ is the squared diffraction vector orthogonal to a Bragg plane; λ denotes the wavelength of the incident X-rays/γ-rays and 2θ is the scattering angle. The B-factors in (3.13) are generated by lattice vibrations orthogonal to the respective Bragg plane. For cubic lattice symmetry, the vibrations are isotropic and one can identify, cf. (3.7), (3.9) and (3.10),

$$B(T)=\frac{(4\pi)^2}{2}\left\langle u_n^2(0)\right\rangle_T,\quad B_2(T)=\frac{(4\pi)^2}{4!}\left(3\left\langle u_n^2(0)\right\rangle_T^2-\left\langle u_n^4(0)\right\rangle_T\right), \tag{3.14}$$

where the averages refer to normal vibrations parallel to a coordinate axis. These B-factors define the first two orders of the cumulant expansion

$$\frac{2M}{Q^2}=\langle u_n^2(0)\rangle_T+\frac{Q^2}{12}\left(3\langle u_n^2(0)\rangle_T^2-\langle u_n^4(0)\rangle_T\right)+\mathrm{O}\left(Q^4\right). \tag{3.15}$$

Conversely, the averaged vibrational amplitudes $\langle u_n^2(0)\rangle_T$ and $\langle u_n^4(0)\rangle_T$ in (3.7) and (3.9) are determined by the $B(T)$ and $B_2(T)$ coefficients in (3.13) and (3.14), which can be inferred from a least-squares fit of the intensity factor $\exp(-2M(Q^2,T))$ at the respective temperature.

4. Temperature-dependent spectral cutoff and varying Debye temperature of elemental cubic crystals

4.1. Extracting the spectral cutoff $\Lambda(T)$ and Debye temperature $\theta(T)$ from heat capacity data and the Debye-Waller B-factor

We write the spectral (i.e. wavenumber) cutoff of the internal energy (2.7) and entropy (2.10) as $\Lambda(T)=n_{\rm at}^{1/3}h(T)$, where $n_{\rm at}$ is the atomic density of the solid and $h(T)$ a dimensionless scale factor. The effective oscillator density is $n_{\rm oscil}=(4\pi/(2\pi)^3)n_{\rm at}h^3$, cf. after (2.8). The internal energy and entropy densities can be converted to molar quantities by multiplying Eqs. (2.8) and (2.11) by V/mol and substituting $n_{\rm at}=n_{a/m}N_{\rm A}{\rm mol}/V$ for the atomic density, where $N_{\rm A}$ is the Avogadro constant and $n_{a/m}$ denotes the number of atoms per molecule or formula unit. The molar internal energy (in units of J/mol) thus reads, cf. (2.8),

$$U(T)=3\frac{4\pi}{(2\pi)^3}n_{a/m}Rh^3T\left(D(d)+\frac{d}{8}\right), \tag{4.1}$$

where $d=\theta(T)/T$ and $R=N_{\rm A}k_{\rm B}=8.314$ J/(K mol) is the gas constant. The molar entropy (in units of J/(K mol)) is found as, cf. (2.11),

$$S(T)=3\frac{4\pi}{(2\pi)^3}n_{a/m}Rh^3\left(\frac{4}{3}D(d)-\frac{1}{3}\log\left(1-\mathrm{e}^{-d}\right)\right). \tag{4.2}$$

The dimensionless factor $h(T)$ defines the spectral cutoff $\Lambda(T)=n_{\rm at}^{1/3}h(T)$. The effective phonon speed is $c_{\rm eff}(T)=k_{\rm B}\theta(T)/(\hbar n_{\rm at}^{1/3}h(T))$, cf. after (2.8). The oscillator mass $m_{\rm eff}(T)$ does not enter in the thermodynamic variables, but emerges in the B-factors and correlation functions as normalization factor of the field amplitudes, cf. (2.18) and (3.1).

The internal energy and entropy are related to the lattice heat capacity $C_V(T)$ (in units of J/(K mol)) by $U(T)=\int_0^T C_V\mathrm{d}T+U_0$ and $S(T)=\int_0^T C_V/T\mathrm{d}T$, where the zero-point internal energy U_0 is an integration constant. In Section 5, an analytic representation of $C_V(T)$ will be obtained from a least-squares fit of a multiply broken power-law density to heat capacity data of copper. The analytic fit function can then be integrated as indicated to find the molar internal energy and entropy. The zero-point energy U_0 can be determined from X-ray/γ-ray or neutron diffraction measurements of the Debye-Waller B-factor at low temperature, cf. (3.14), (4.14) and Section 5.

Once $U(T)$ and $S(T)$ are known, one can extract the varying Debye temperature $\theta(T)$ and the spectral cutoff factor $h(T)$ from (4.1) and (4.2). The varying Debye temperature $\theta(T)=Td(T)$ is obtained by solving, cf. Ref. [9],

$$\frac{3}{4}\frac{TS(T)}{U(T)}=\Delta(d),\quad\Delta(d):=1-\frac{2\log(1-\mathrm{e}^{-d})+d}{8D(d)+d}, \tag{4.3}$$

for $d(T)$. The Debye function $D(d)$ is defined in (2.8). $\Delta(d)$ is an invertible function, monotonously decreasing from infinity at $d=0$ to zero at $d=\infty$. The Debye temperature is thus unambiguously determined by the inverse of $\Delta(d)$,

$$\theta(T)=T\Delta^{-1}\left(\frac{3}{4}\frac{TS(T)}{U(T)}\right). \tag{4.4}$$

The spectral cutoff $\Lambda(T) = n_{\rm at}^{1/3} h(T)$ is obtained by solving (4.1) for $h(T)$,

$$h(T) = \left(\frac{1}{3}\frac{(2\pi)^3}{4\pi}\frac{1}{n_{a/m}RT}\frac{U(T)}{D(d)+d/8}\right)^{1/3}, \tag{4.5}$$

with $U(T)$ and $d = \theta(T)/T$ in (4.4) substituted.

The cumulant $\widehat{\kappa}_T = 3\langle u_n^2(0)\rangle_T^2 - \langle u_n^4(0)\rangle_T$ in (3.10) can be assembled as, cf. (3.11) and (3.12),

$$\widehat{\kappa}_T = \left(\frac{3}{m_{\rm eff}}\frac{\hbar^2 T}{k_{\rm B}\theta^2}\right)^2\left(D_1^2(d) + \frac{1}{2}dD_1(d) + \frac{d^2}{8}\right), \tag{4.6}$$

where $D_1(d)$ is a Debye function defined in (2.17). The mean-squared vibrations $\langle u_n^2(0)\rangle_T$ in (2.19) and the cumulant (4.6) define the Debye-Waller B-factors (3.14), that is $B(T) = 8\pi^2\langle u_n^2(0)\rangle_T$ and $B_2(T) = 2\pi^2\widehat{\kappa}_T/3$. Asymptotic limits $d = \theta(T)/T \to 0, \infty$ of the functions derived in this section are listed in Appendix B.

4.2. High-temperature asymptotics of the spectral cutoff, Debye temperature and B-factors

In the high-temperature regime, the molar lattice heat capacity approaches the classical limit $C_V(T\to\infty) \sim c_{V\infty}, c_{V\infty} := 3n_{a/m}R$, where $n_{a/m}$ denotes the number of atoms per molecule or formula unit and R the gas constant. Since $U(T) = \int_0^T C_V {\rm d}T + U_0$ and $S(T) = \int_0^T C_V/T {\rm d}T$, the asymptotic limits of the internal energy and entropy are $U(T\to\infty) \sim c_{V\infty}T$ and $S(T\to\infty) \sim c_{V\infty}\log T + s_{V\infty}$, with constant $s_{V\infty}$. Thus,

$$\frac{3}{4}\frac{TS(T)}{U(T)} \sim \frac{3}{4}\left(\log T + \frac{s_{V\infty}}{c_{V\infty}}\right), \tag{4.7}$$

where we can replace the left-hand side by the limit $\Delta(d\to 0)$ in (B.3). Solving this equation for $d = \theta(T)/T$, we find the constant asymptotic limit of the Debye temperature, $\theta_{T\to\infty} \sim \exp(4/3 - s_{V\infty}/c_{V\infty})$. The asymptotic limit of the spectral cutoff $\Lambda(T) = n_{\rm at}^{1/3}h(T)$ is obtained by substituting $U \sim c_{V\infty}T$ for $U_{d\to 0}$ in (B.1) and solving for h, which gives $h_{T\to\infty} \sim (6\pi^2)^{1/3}$.

Substitution of the limit $\theta_{T\to\infty}$ into the mean-squared vibration $\langle u_n^2(0)\rangle_{T,d\to 0}$ in (B.4) and the cumulant $\widehat{\kappa}_{T,d\to 0}$ in (B.5) gives

$$\left\langle u_n^2(0)\right\rangle_{T\to\infty} \sim \frac{3}{m_{\rm eff}(T)}\frac{\hbar^2 T}{k_{\rm B}}\exp\left(-\frac{8}{3} + 2\frac{s_{V\infty}}{c_{V\infty}}\right), \quad \widehat{\kappa}_{T\to\infty} \sim \left\langle u_n^2(0)\right\rangle_{T\to\infty}^2, \tag{4.8}$$

which defines the high-temperature limit of the B-factors, cf. after (4.6).

4.3. Low-temperature limits and zero-point internal energy

Reasoning analogous to Section 4.2 applies in the low-temperature regime. The lattice heat capacity scales as $C_V(T\to 0) \sim c_{V0}T^3$, with constant amplitude c_{V0}, so that the internal energy converges to its zero-point limit, $U(T\to 0) \sim U_0$, and the entropy scales as $S(T\to 0) \sim c_{V0}T^3/3$, cf. after (4.2). Hence,

$$\frac{3}{4}\frac{TS(T)}{U(T)} \sim \frac{1}{4}\frac{c_{V0}T^4}{U_0}, \tag{4.9}$$

where we substitute $\Delta(d\to\infty)$, cf. (B.3), on the left-hand side. Solving this equation for $d = \theta(T)/T$, gives

$$\theta_{T\to 0} \sim \left(\frac{32\pi^4}{15}\frac{U_0}{c_{0V}}\right)^{1/4} \tag{4.10}$$

as finite low-temperature limit of the Debye temperature. The low-temperature limit of the cutoff factor $h_{T\to 0}$ is also finite, obtained by substituting $U \sim U_0$ for $U_{d\to\infty}$ in (B.1) and solving for h,

$$h_{T\to 0} \sim \left(\frac{(2\pi)^3}{4\pi}\frac{8}{3}\frac{U_0}{n_{a/m}R}\frac{1}{\theta_{T\to 0}}\right)^{1/3} = \left(\frac{5}{2\pi^2}\frac{c_{0V}}{n_{a/m}R}\right)^{1/3}\theta_{T\to 0}, \tag{4.11}$$

with $\theta_{T\to 0}$ in (4.10). The zero-temperature limits of the B-factors (see after (4.6)) are determined by the averages

$$\langle u_n^2(0)\rangle_{T=0} = \frac{3}{m_{\rm eff}(0)}\frac{\hbar^2}{k_{\rm B}}\frac{1}{4}\left(\frac{15}{32\pi^4}\frac{c_{V0}}{U_0}\right)^{1/4}, \tag{4.12}$$

$$\widehat{\kappa}_{T=0} = \left(\frac{3}{m_{\rm eff}(0)}\frac{\hbar^2}{k_{\rm B}}\right)^2\frac{1}{8}\left(\frac{15}{32\pi^4}\frac{c_{V0}}{U_0}\right)^{1/2}, \tag{4.13}$$

derived from the mean-squared amplitude $\langle u_n^2(0)\rangle_{T,d\to\infty}$ in (B.4), the cumulant $\widehat{\kappa}_{T,d\to\infty}$ in (B.5) and $\theta_{T\to 0}$ in (4.10). The effective oscillator mass of monatomic crystals at zero temperature is identified with the atomic mass, $m_{\rm eff}(0) = m$. Solving Eq. (4.12) for U_0 gives

$$U_0 = \left(\frac{3}{m}\frac{\hbar^2}{k_{\rm B}}\frac{1}{4}\right)^4\frac{15}{32\pi^4}\frac{c_{V0}}{\langle u_n^2(0)\rangle_{T=0}^4}, \tag{4.14}$$

so that the zero-point internal energy of the lattice vibrations can be inferred from a measurement of the Debye-Waller factor $B(0) = 8\pi^2\langle u_n^2(0)\rangle_{T=0}$ at a temperature close to zero, since the mean-squared vibration $\langle u_n^2(0)\rangle_T$ is nearly constant at low temperature, cf. Section 5. The constant c_{V0} in (4.14) is the empirical amplitude of the cubic low-temperature scaling of the lattice heat capacity, see the beginning of this section. We may write (4.14) as

$$U_0\left[{\rm J/mol}\right] = 8.4309\times 10^3\frac{c_{V0}\left[{\rm J/(K^4\ mol)}\right]}{\left(m\left[{\rm u}\right]\langle u_n^2(0)\rangle_{T=0}[{\rm \AA}^2]\right)^4}, \tag{4.15}$$

where we used $\hbar^2/({\rm u}k_{\rm B}) = 48.509\ {\rm \AA^2 K}$.

5. Effective correlation functions of lattice vibrations in copper

We start with a least-squares fit to the data set [33] of the lattice heat capacity of copper, depicted in the double-logarithmic plot in Fig. 1, by employing a multiply broken power law [34–36] for the molar heat capacity,

$$C_V(T) = b_0T^3\left(1 + (T/b_1)^{\beta_1/\eta_1}\right)^{\eta_1}\frac{1}{\left(1 + (T/b_2)^{\beta_2/\eta_2}\right)^{\eta_2}}. \tag{5.1}$$

The amplitudes $b_1 < b_2$ and exponents β_1, η_1 and β_2, η_2 are positive, and $\beta_2 = 3 + \beta_1$, $b_0 = 3Rb_1^{\beta_1}/b_2^{\beta_2}$, so that the classical limit $C_V(T\to\infty) \sim 3R$ is recovered. The low-temperature limit is $C_V(T\to 0) \sim b_0T^3$, and the units used are C_V[J/(K mol)], b_0[J/(K^4 mol)] and b_1[K], b_2[K].

The parameters $b_0, b_1, b_2, \eta_1, \eta_2$ and β_1, β_2 are recorded in Table 1. The independent parameters varied in the χ^2 fit are $b_1, \beta_1, \eta_1, \eta_2$. The amplitude b_0[J/(K^4 mol)] $= 4.7369\times 10^{-5}$ is taken as experimental input (so that $c_{V0} = b_0$ and $n_{a/m} = 1$ in Section 4.3) and $\beta_2 = 3 + \beta_1$, $b_2 = (3Rb_1^{\beta_1}/b_0)^{1/\beta_2}$. Multiply broken power laws composed of factors $(1 + (T/b_i)^{\beta_i/|\eta_i|})^{\eta_i}$ are quite efficient to fit data sets extending over several logarithmic decades. In (5.1), there are three successive power laws, $\propto T^3$, $T^{3+\beta_1}$, 1, in the intervals $T < b_1$, $b_1 < T < b_2$ and $b_2 < T$, respectively. The exponents η_i determine the curvature in the transitional regions around the break points b_i between the straight power-law slopes in log-log plots.

In Fig. 1, we have also indicated the Debye approximation,

$$C_{\rm D}(T) = 9n_{a/m}R\left[4D(\theta_{\rm D}/T) - \frac{\theta_{\rm D}/T}{{\rm e}^{\theta_{\rm D}/T} - 1}\right], \quad \theta_{\rm D} = \left(\frac{12}{5}\pi^4\frac{n_{a/m}R}{b_0}\right)^{1/3}, \tag{5.2}$$

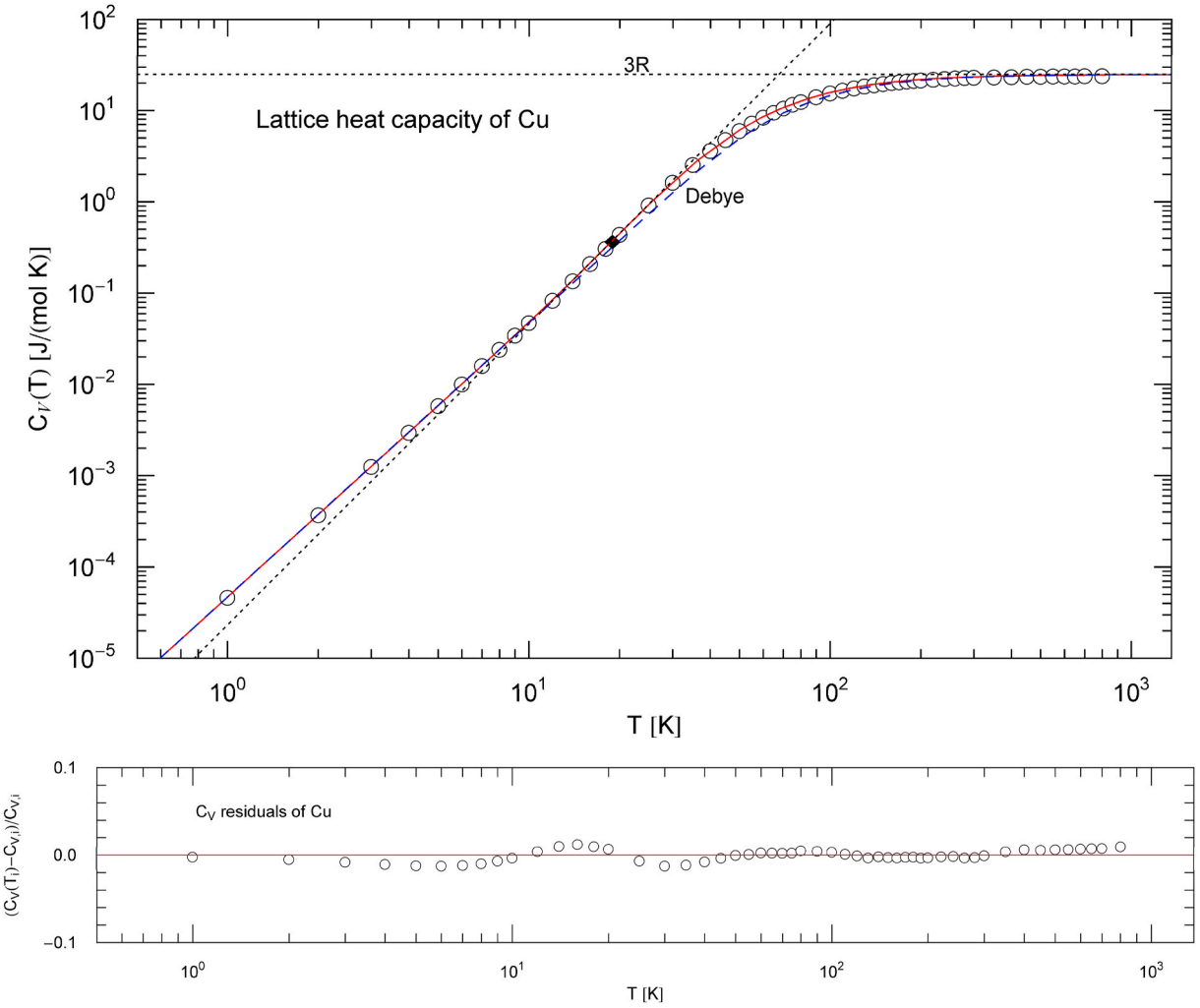

Fig. 1. Lattice heat capacity of copper. Data points (circles) from Ref. [33]. The least-squares χ^2 fit (solid red curve) is performed with the multiply broken power-law density $C_V(T)$ in (5.1), the fitting parameters are recorded in Table 1. The classical $3R$ limit is indicated by the horizontal black dotted line. The blue dashed curve is the Debye approximation (5.2) with constant Debye temperature $\theta_D = 344.9$ K. The black dotted straight line depicts the tangent $\propto T^\kappa$ at the inflection point of this log-log plot (black diamond, $T = 18.93$ K, $C_V = 0.377$ J/(mol K)) with slope $\kappa = 3.295$. Residuals of the χ^2 fit are depicted in the lower panel.

Table 1
Fitting parameters of the lattice heat capacity $C_V(T)$ of copper. The recorded amplitudes b_i and exponents β_i, η_i define the multiply broken power-law density (5.1) used for the χ^2 fit depicted in Fig. 1. $\chi^2 = \sum_{i=1}^N (C_V(T_i) - C_{Vi})^2 / C_{Vi}^2$ denotes the minimum of the least-squares functional. The data points used are recommended values from Ref. [33]; no error bounds are given in this reference, but the data are corrected for thermal expansion. The degrees of freedom (dof: number N of data points (T_i, C_{Vi}) minus number of independent fitting parameters), the standard error of the fit, SE $= (\sum_{i=1}^N (C_V(T_i) - C_{Vi})^2/N)^{1/2}$, and the determination coefficient $R^2 = 1 - \sum_{i=1}^N (C_V(T_i) - C_{Vi})^2/(N\sigma^2)$, with sample variance $\sigma^2 = \sum_{i=1}^N (C_{Vi} - \overline{C}_V)^2/N$ and mean $\overline{C}_V = \sum_{i=1}^N C_{Vi}/N$, are also listed.

b_0[J/(K^4 mol)]	b_1[K]	b_2[K]	β_1	β_2	η_1	η_2	χ^2	dof	SE	$1 - R^2$
4.7369×10^{-5}	19.248	40.205	2.8404	$3 + \beta_1$	1.1640	3.0031	2.17×10^{-3}	$53 - 4$	8.08×10^{-2}	6.53×10^{-5}

with Debye function $D(d)$ in (2.8) and $n_{a/m} = 1$ (number of atoms per formula unit) for monatomic crystals. The constant Debye temperature of copper is $\theta_D = 344.92$ K, and the constant spectral cutoff $h_D = (6\pi^2)^{1/3}$ is required to recover the classical high-temperature limit, cf. Section 4.2. In contrast to the Debye approximation (5.2), the empirical lattice heat capacity of copper in log-log representation has an inflection point in the crossover region between the low- and high-temperature regimes, see Fig. 1; the tangent of the regressed heat capacity $C_V(T)$ at the inflection point is shown as black dotted straight line. The zero-point internal energy of the Debye approximation is $U_{0,D} = 9n_{a/m}R\theta_D/8$, cf. (B.1), with gas constant $R = 8.314$ J/(K mol), so that $U_{0,D} = 3226$ J/mol for copper.

In the previous sections, we explained how to model empirical deviations from the Debye heat capacity (5.2) by a temperature-dependent Debye temperature $\theta(T)$ and spectral cutoff $h(T)$. In this case, the zero-point internal energy U_0 is not any more determined by the Debye temperature but is an integration constant (see after (4.2)) to be extracted from the zero-temperature limit of the experimental Debye-Waller $B(T)$-factor. The empirical temperature evolution of the mean-squared atomic vibration $\langle u_n^2(0)\rangle_T$ of copper (which gives the B-factor $8\pi^2\langle u_n^2(0)\rangle_T$, cf. after (4.6)) was obtained in Ref. [37] by least-squares

regression from Mössbauer γ-ray diffraction data, based on the fit function

$$\left\langle u_n^2(0)\right\rangle_T = \frac{3}{m}\frac{\hbar^2 T}{k_B\theta_X^2}\left(D_1(d_X)+\frac{d_X}{4}\right)+m_2T^2+m_3T^3, \tag{5.3}$$

with $d_X = \theta_X/T$, atomic mass m, and Debye function $D_1(d)$ in (2.17). The constant X-ray Debye temperature $\theta_X \approx (340\pm 12)$ K (in this case obtained by using a Mössbauer 46 keV γ-ray source) and the constants $m_2 \approx (6.3\pm 1.3)\times 10^{-9}\text{Å}^2/\text{K}^2$ and $m_3 \approx 0$ were inferred from the data fit in Ref. [37]. Similar values were obtained in Ref. [38], also by Mössbauer spectroscopy. The data sets used to infer (5.3) were corrected for thermal expansion [39–41], so that $\langle u_n^2(0)\rangle_T$ represents the temperature evolution at constant volume, assumed throughout this paper. The zero-temperature limit of (5.3) is $\langle u_n^2(0)\rangle_{T=0} = 3\hbar^2/(4mk_B\theta_X)$, cf. (B.4), which can be written as $\langle u_n^2(0)\rangle_{T=0}[\text{Å}^2] = 36.382/(m[\text{u}]\theta_X[\text{K}])$, using $\hbar^2/(\text{u}k_B) = 48.509$ Å^{2}K. For copper, $m[\text{u}] = 63.546$, so that $\langle u_n^2(0)\rangle_{T=0} = 1.6839\times 10^{-3}\text{Å}^2$. The zero-point energy U_0 is calculated by substituting this $\langle u_n^2(0)\rangle_{T=0}$ into (4.15). Also needed in (4.15) is the amplitude $c_{V0}[\text{J}/(\text{K}^4\text{ mol})]$ of the cubic low-temperature scaling of the heat capacity, which can be identified with b_0 in Table 1 according to (5.1). We find $U_0 = 3046$ J/mol, somewhat lower than the zero-point energy of the Debye model, cf. after (5.2).

The temperature dependence of the Debye temperature $\theta(T)$, cf. Fig. 2, and the spectral cutoff $\Lambda(T) = n_{\text{at}}^{1/3}h(T)$, cf. Fig. 3, can be calculated by way of (4.4) and (4.5), with the internal energy $U(T) = \int_0^T C_V\text{d}T + U_0$ and entropy $S(T) = \int_0^T C_V/T\text{d}T$ as empirical input functions, using the regressed heat capacity $C_V(T)$ in (5.1) and the zero-point energy U_0 as specified above. The effective phonon speed defining the dispersion relation is $c_{\text{eff}}(T) = k_B\theta(T)/(\hbar n_{\text{at}}^{1/3}h(T))$, cf. after (4.2); for copper, $c_{\text{eff}}(T)[\text{cm}/\text{s}] = 2979\,\theta(T)[\text{K}]/h(T)$, see Fig. 4, calculated with the atomic density $n_{\text{at}}[1/\text{Å}^3] = 0.0849$, based on a molar mass of 63.546 g/mol and a mass density of 8.96 g/cm^3.

Once the varying Debye temperature $\theta(T)$ and spectral cutoff $h(T)$ are known, the effective oscillator mass $m_{\text{eff}}(T)$ is obtained by substituting the regressed function (5.3) (representing the experimental mean-squared vibration $\langle u_n^2(0)\rangle_T$) into (2.19) and solving this equation for $m_{\text{eff}}(T)$,

$$m_{\text{eff}}(T)[\text{u}] = \frac{145.53}{\langle u_n^2(0)\rangle_T[\text{Å}^2]}\frac{T[\text{K}]}{\theta^2(T)[\text{K}]}\left(D_1(d(T))+\frac{d(T)}{4}\right), \tag{5.4}$$

where $d(T) = \theta(T)/T$ and, cf. (5.3),

$$\left\langle u_n^2(0)\right\rangle_T[\text{Å}^2] = \frac{145.53}{m[\text{u}]}\frac{T[\text{K}]}{\theta_X^2[\text{K}]}\left(D_1(d_X)+\frac{d_X}{4}\right)+m_2T^2+m_3T^3. \tag{5.5}$$

The fitting parameters θ_X, m_2, m_3 in (5.5) are stated after (5.3), $d_X = \theta_X/T$, and $m = 63.546$ u is the atomic mass of copper. The numerical factor in (5.4) and (5.5) stems from $3\hbar^2/(\text{u}k_B) = 145.53$ Å^{2}K. At zero temperature, the effective oscillator mass $m_{\text{eff}}(T)$, plotted in Fig. 5, coincides with the atomic mass, $m_{\text{eff}}(0) = m$, and $\theta(0) = \theta_X$, cf. (4.10) and after (5.3).

The Debye-Waller factor $B(T)$, cf. (2.19) and after (4.6),

$$B(T)[\text{Å}^2] = 8\pi^2\frac{145.53}{m_{\text{eff}}(T)[\text{u}]}\frac{T[\text{K}]}{\theta^2(T)[\text{K}]}\left(D_1(d(T))+\frac{d(T)}{4}\right), \tag{5.6}$$

coincides with the regressed experimental B-factor $8\pi^2\langle u_n^2(0)\rangle_T$ in (5.5) and is plotted in Fig. 6, together with the B-factor $B_D(T)$ of the Debye model. $B_D(T)$ is defined by the mean-squared vibration $\langle u_n^2(0)\rangle_T$ as stated in (5.5), but with $m_2 = m_3 = 0$ and θ_X replaced by θ_D. (The constant caloric Debye temperature θ_D obtained from a least-squares fit based on $C_D(T)$ in (5.2) usually deviates from the Debye temperature θ_X obtained

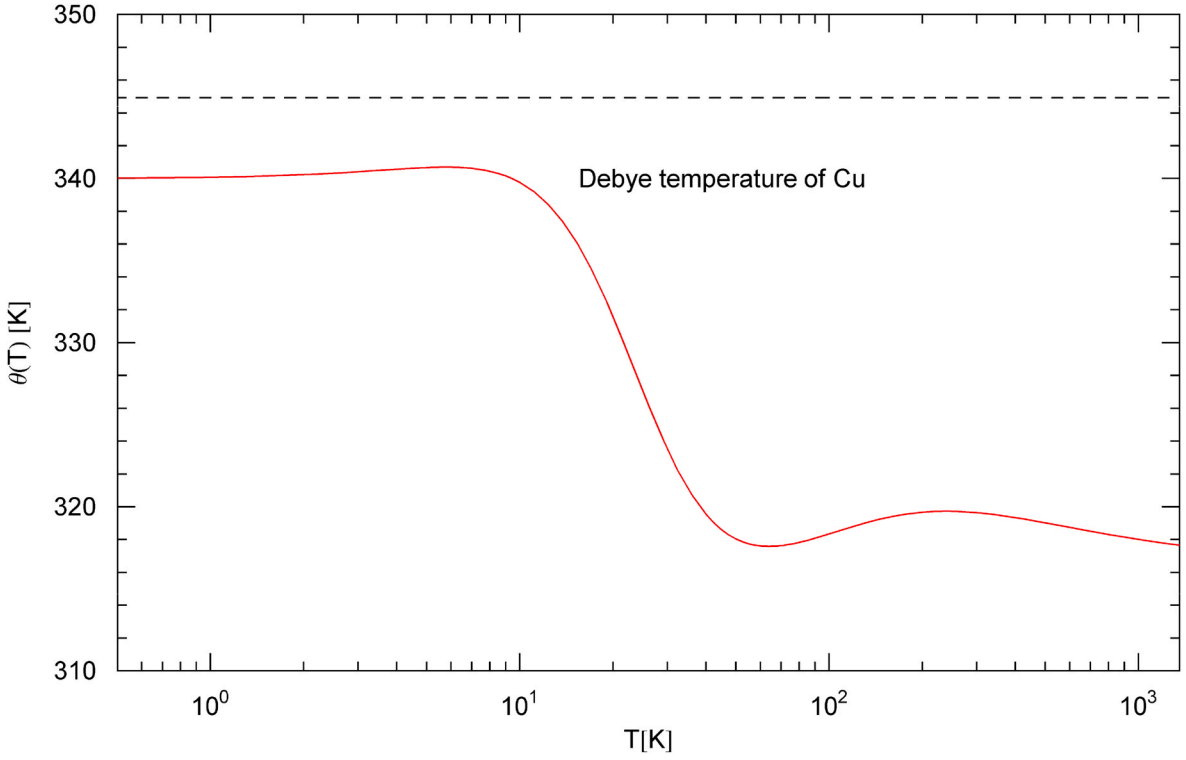

Fig. 2. Varying Debye temperature of copper. The temperature dependence of the Debye temperature $\theta(T)$ (red solid curve) is calculated from the temperature variation of the internal energy and entropy, cf. (4.4) and after (5.3). $\theta(T)$ approaches constant limit values at low and high temperature, cf. Sections 4.2 and 4.3; the constant high-temperature limit is not attained within the solid phase. (In the figures, the temperature range is cut off at the melting point of copper, at 1357.8 K.) The black dashed straight line indicates the constant Debye temperature $\theta = 344.9$ K, used in the Debye approximation (5.2) of the heat capacity depicted in Fig. 1.

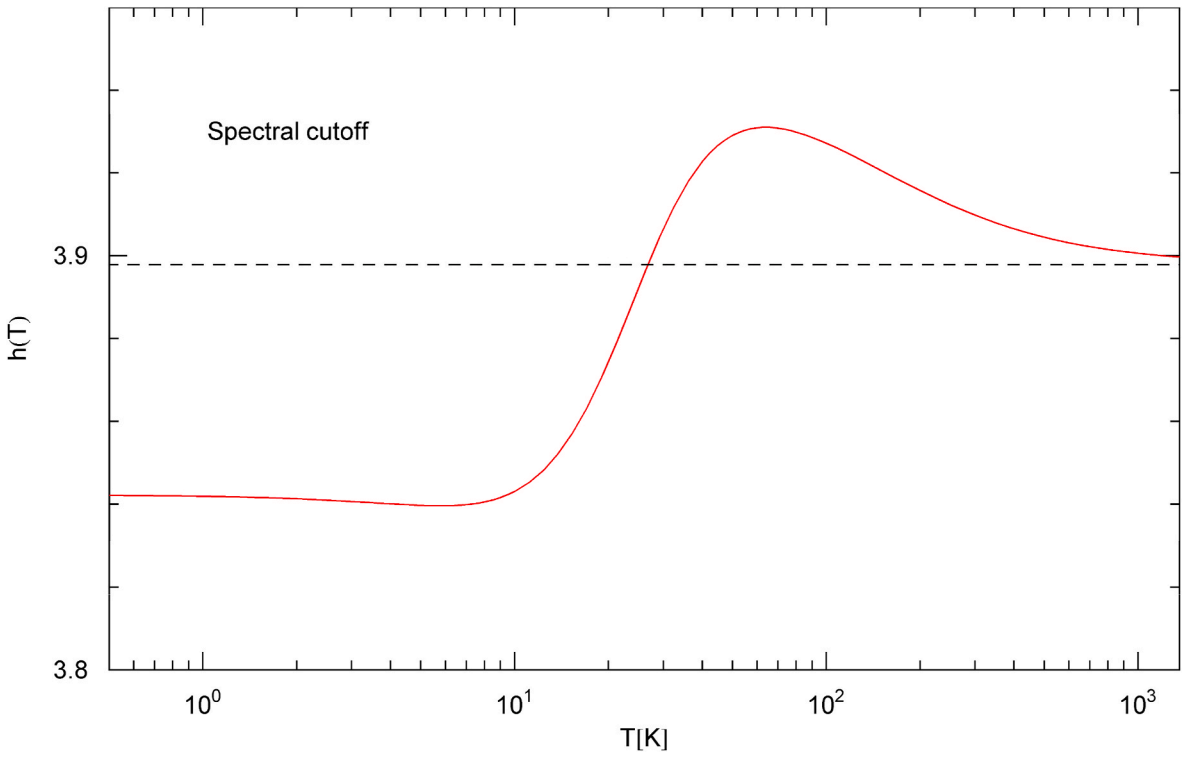

Fig. 3. Spectral cutoff of the thermodynamic variables of copper. The cutoff factor $\Lambda(T) = n_{\rm at}^{1/3}h(T)$ in the spectral representation of the thermodynamic functions in (2.7)–(2.11) depends on the atomic density of copper, $n_{\rm at} = 0.0849/\text{Å}^3$, cf. after (5.3), and a dimensionless cutoff factor $h(T)$ (red solid curve), cf. the beginning of Section 4.1. $h(T)$ is calculated from the internal energy $U(T)$ and the Debye temperature $\theta(T)$ via (4.5), see also Section 5. The low- and high-temperature limits of $h(T)$ are constant, cf. Sections 4.2 and 4.3. At high temperature, $h(T)$ converges to the constant cutoff factor of the Debye approximation, $h_{\rm D} = (6\pi^2)^{1/3}$ (black dashed line), cf. after (5.2). In the low-temperature regime, $h(T)$ depends on the zero-point internal energy U_0, cf. (4.11), inferred from the experimental Debye-Waller B-factor, cf. Section 5.

from the fit (5.3) of the mean-squared atomic displacement measured by diffraction.) One can also recover $B_{\rm D}(T)$ from $B(T)$ in (5.6), by putting $m_{\rm eff}(T) = m$ (atomic mass) and $\theta(T) = \theta_{\rm D}$, $d(T) = \theta_{\rm D}/T$. At zero temperature, $B_{\rm D}(0)/B(0) = \theta_{\rm X}/\theta_{\rm D}$, since $D_1(d\to\infty) \sim \pi^2/(6d)$. At high temperature, $B_{\rm D}(T)\propto T$, since $D_1(d\to 0) \sim 1$, see Fig. 6.

The Debye-Waller intensity factor e^{-2M}, where $M = (Q^2/(4\pi)^2)(B + B_2Q^2 + \cdots)$, cf. (3.13), also depends on the second-order coefficient $B_2 = 2\pi^2\widehat{\kappa}_T/3$, defined by the cumulant $\widehat{\kappa}_T = 3\langle u_n^2(0)\rangle_T^2 - \langle u_n^4(0)\rangle_T$, cf. after (4.6). The temperature variation of this factor reads, cf. (4.6),

$$B_2(T)\left[\text{Å}^4\right] = \frac{2\pi^2}{3}\left(\frac{145.53}{m_{\rm eff}(T)}\,\frac{T}{\theta^2(T)}\right)^2\left(D_1^2(d) + \frac{1}{2}dD_1(d) + \frac{d^2}{8}\right), \tag{5.7}$$

where $m_{\rm eff}(T)[\text{u}]$ is in atomic mass units, and $T[\text{K}]$, $\theta(T)[\text{K}]$ and $d(T) = \theta(T)/T$. The Debye approximation $B_{2,\rm D}(T)$ of $B_2(T)$ is found by replacing $m_{\rm eff}(T)$ in (5.7) by the atomic mass $m[\text{u}] = 63.546$ of copper and $\theta(T)$ by the constant Debye temperature $\theta_{\rm D} = 344.92$ K, cf. after (5.2). At high temperature, $B_{2,\rm D}(T)\propto T^2$, and $B_{2,\rm D}(0)/B_2(0) = \theta_{\rm X}^2/\theta_{\rm D}^2$ at zero temperature, see after (B.5) and (5.6) and Fig. 6.

The two-point correlation function of lattice vibrations, $C^{(2)}(r,T) = \langle\widehat{A}(r)\rangle_T + \langle\widehat{B}(r)\rangle_T/2$, cf. (3.6), and the reduced four-point correlation $C^{(4)}(r,T) = \langle\widehat{A}(r)\rangle_T^2 + \langle\widehat{B}(r)\rangle_T\langle\widehat{A}(r)\rangle_T$, cf. (3.3), are assembled with the averages calculated in (3.11) and (3.12),

$$\left\langle\widehat{A}(r)\right\rangle_T = \frac{145.53}{m_{\rm eff}(T)}\,\frac{T^2}{\theta^3(T)}\int_0^{\theta/T}\frac{\sin(zT\Lambda r/\theta)}{zT\Lambda r/\theta}\,\frac{z\mathrm{d}z}{\mathrm{e}^z-1}, \tag{5.8}$$

$$\left\langle\widehat{B}(r)\right\rangle_T = \frac{145.53}{m_{\rm eff}(T)}\,\frac{1}{\theta(T)}\,\frac{1}{(\Lambda r)^2}(1-\cos(\Lambda r)\,). \tag{5.9}$$

The units used here are stated after (5.7) and $\langle\widehat{A}(r)\rangle_T[\text{Å}^2]$, $\langle\widehat{B}(r)\rangle_T[\text{Å}^2]$, $\Lambda(T)[1/\text{Å}]$, $r[\text{Å}]$, and $\Lambda(T) = n_{\rm at}^{1/3}h(T)$, where $n_{\rm at}[1/\text{Å}^3]$ is the atomic density and $h(T)$ is dimensionless, cf. after (5.3). For copper, $n_{\rm at}^{1/3} = 0.43953/\text{Å}$. The asymptotic limit of $\langle\widehat{A}(r)\rangle_T$ for large Λr is stated in (A.11), where we substitute $3\hbar^2/(\text{u}k_{\rm B}) = 145.53\ \text{Å}^2\text{K}$ and use the units enumerated above. $C^{(2)}(r,T)$ measures the correlation of atomic displacements as a function of distance and temperature, cf. (2.20), and $C^{(4)}(r,T)$ correlates fluctuations around the mean-squared displacement, cf. (3.2). In Fig. 7, these correlations are plotted for copper, at selected temperatures representing the high, intermediate and low temperature regimes. Asymptotically, $\langle\widehat{A}(r)\rangle_T \propto 1/r$ and $\langle\widehat{B}(r)\rangle_T = \text{O}(1/r^2)$. In the opposite short-distance regime $\Lambda r << 1$, $\langle\widehat{A}(r)\rangle_T$ and $\langle\widehat{B}(r)\rangle_T$ are nearly constant and converge to the limits $\langle\widehat{A}(0)\rangle_T$ and $\langle\widehat{B}(0)\rangle_T$ stated in (3.11) and (3.12). At high temperature, $\langle\widehat{A}(r)\rangle_T$ overpowers the oscillatory $\langle\widehat{B}(r)\rangle_T$ also in the short-distance and crossover regimes, so that the correlations $C^{(2)}(r,T)$ and $C^{(4)}(r,T)$ are non-oscillatory like $\langle\widehat{A}(r)\rangle_T$. At low temperature, $\langle\widehat{B}(r)\rangle_T$ dominates $\langle\widehat{A}(r)\rangle_T$ at small distances, which causes the oscillations of the correlation functions in the crossover region depicted in Fig. 7, since $\langle\widehat{B}(r)\rangle_T$ is oscillatory in the crossover and long-range regimes.

6. Heat capacity and Debye-Waller factors of anisotropic compounds

The purpose of this section is to explain how the phenomenological field theory developed in this paper for cubic elemental crystals can be extended to cover the (anisotropic) compounds mentioned in the

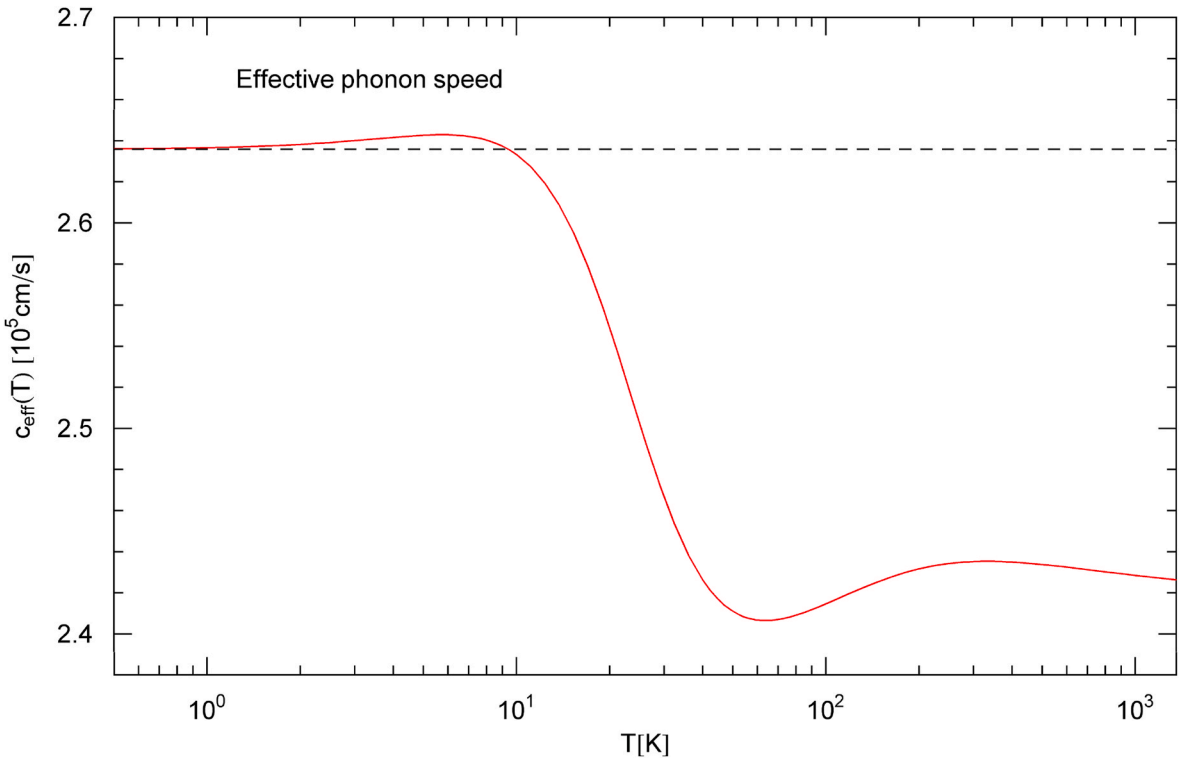

Fig. 4. Effective phonon speed of copper. $c_{\rm eff}(T)$ (red solid curve) is calculated from the Debye temperature $\theta(T)$ in Fig. 2 and the spectral cutoff $h(T)$ in Fig. 3, cf. after (5.3), and converges to finite limit values at low and high temperature (since $\theta(T)$ and $h(T)$ admit finite limits). At low temperature, $c_{\rm eff}(T)$ approaches the constant averaged phonon speed of the Debye approximation (depicted as black dashed straight line). The constant high-temperature limit of $c_{\rm eff}(T)$ is not attained below the melting point.

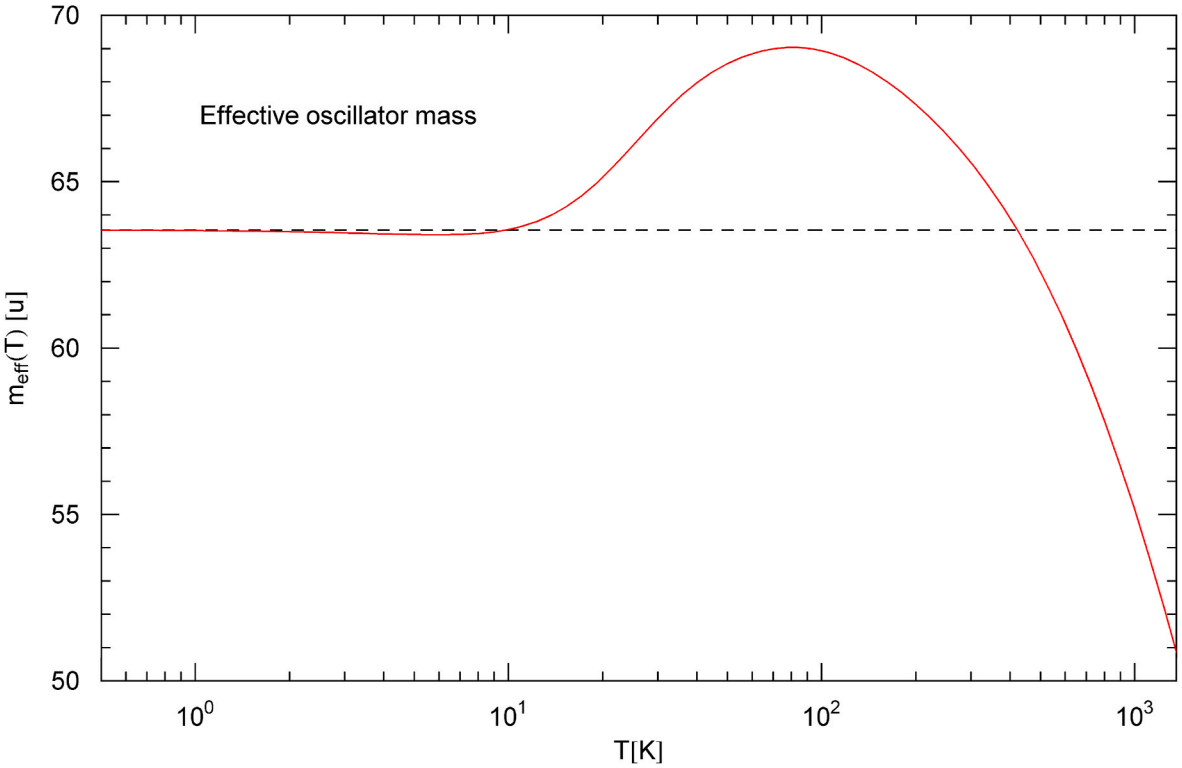

Fig. 5. Effective oscillator mass of copper. Depicted is $m_{\rm eff}(T)$ in (5.4) (solid red curve), extracted from the measured temperature variation of the Debye-Waller B-factor and Debye temperature $\theta(T)$, cf. Section 5 and the caption of Fig. 6. The horizontal dashed line indicates the atomic mass of copper, which is the low-temperature limit of $m_{\rm eff}(T)$. The temperature range is cut off at the melting point.

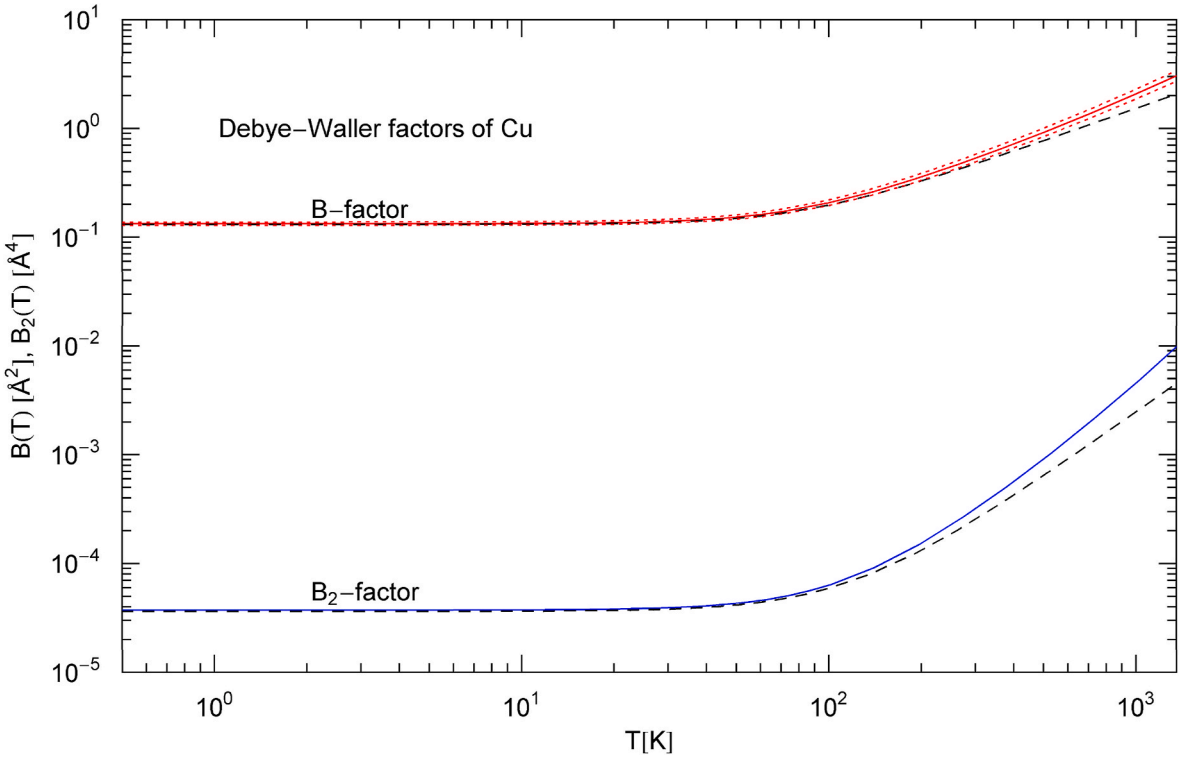

Fig. 6. Debye-Waller B-factors of copper. The red solid curve depicts $B(T)$ in (5.6), the dotted red curves indicate the experimental 1σ error band (obtained from the error estimates of the fitting parameters in Ref. [37]), and the blue solid curve shows the second-order Debye-Waller factor $B_2(T)$ in (5.7). The Debye approximations of $B(T)$ and $B_2(T)$ are indicated as black dashed curves, increasing linearly/quadratically at high T, cf. after (5.6) and (5.7). These approximations underestimate the B-factors at high temperature, and they also slightly deviate from $B(T)$ and $B_2(T)$ at low temperature. The effective oscillator mass $m_{\rm eff}(T)$ depicted in Fig. 5 is obtained by equating $B(T)$ in (5.6) to the experimental B-factor $8\pi^2\langle u_n^2(0)\rangle_T$ in (5.5), where $\langle u_n^2(0)\rangle_T$ is a least-squares fit to the mean-squared atomic displacement measured by (Mössbauer) γ-ray diffraction in Ref. [37]. The zero-point internal energy U_0 is obtained from the zero-temperature limit of $B(T)$, cf. (4.14) and after (5.3).

Introduction.

6.1. Empirical modeling of the thermodynamic variables of anisotropic compounds

Lattice vibrations of compounds are described by a multiplet of real massless scalar fields $u_j(\mathbf{x},t)$, coupled to permeability tensors $g_j^{\alpha\beta}$ with components $g_j^{00}=-\mu_j^{1/2}\varepsilon_j$, $g_j^{ab}=\delta^{ab}/\mu_j^{1/2}$ and $g_j^{a0}=g_j^{0a}=0$, where $\varepsilon_j(T)$ and $\mu_j(T)$ are positive permeabilities depending on temperature, cf. Section 2.1 and the beginning of Section 3. The field components and permeability tensors are indexed by the multi-index $j=(n,\Xi)$. The index $\Xi=1,\ldots,N$ labels the atomic species in the formula unit. Each atom of species Ξ is represented by three one-dimensional harmonic oscillators vibrating parallel to the coordinate axes labeled $n=1,2,3$ (normal vibrations). The field component $u_{j=(n,\Xi)}(\mathbf{x},t)$ is generated by the normal vibrations of atomic species Ξ parallel to the coordinate axis labeled n. The coordinate system can be arbitrarily chosen; for instance, in the case of hexagonal lattice symmetry, one will conveniently choose the hexagonal axis and two perpendicular axes in the basal plane. Instead of a vector field coupled to an anisotropic permeability tensor, we use, for each atomic species, a scalar triplet whose components are coupled to different isotropic permeability tensors, cf. the beginning of Section 3.

The Lagrangian of the field multiplet reads $L=-\sum_j g_j^{\alpha\beta}\partial_\alpha u_j\partial_\beta u_j/2$, leading to the wave equations $(\Delta-\mu_j\varepsilon_j\partial_t^2)u_j=0$ for the field components. The energy density is $\rho(\mathbf{x},t)=\sum_j(\mu_j^{1/2}\varepsilon_j(\partial_t u_j)^2/2+(\nabla u_j)^2/(2\mu_j^{1/2}))$, cf. (2.1). The wave equations are solved by the Fourier modes $u_j(\mathbf{x},t)=\phi_{j,\mathbf{k}}e^{i(\mathbf{kx}-\omega_{j,\mathbf{k}}t)}$ with temperature-dependent dispersion relation $\omega_{j,\mathbf{k}}=c_{{\rm eff},j}(T)k$, where $c_{{\rm eff},j}=1/\sqrt{\varepsilon_j(T)\mu_j(T)}$ is the effective phonon speed of the field component $j=(n,\Xi)$. The Fourier decomposition of $u_j(\mathbf{x},t)$ reads as in (3.1), with index n replaced by the multi-index $j=(n,\Xi)$ and the frequencies $\omega_{\mathbf{k}}$ by $\omega_{j,\mathbf{k}}$. By performing the quantization outlined in Section 2.1 and after (3.1), replacing the Fourier amplitudes in (3.1) by annihilation/creation operators, $\phi_{j,\mathbf{k}}\to a_{j,\mathbf{k}}/\sqrt{\mu_j^{1/2}\varepsilon_j\omega_{j,\mathbf{k}}}$, $\phi_{j,\mathbf{k}}^*\to a_{j,\mathbf{k}}^\dagger/\sqrt{\mu_j^{1/2}\varepsilon_j\omega_{j,\mathbf{k}}}$, we find the energy density $\rho(\mathbf{x})=(2L^3)^{-1}\sum_{j,\mathbf{k}}\omega_{j,\mathbf{k}}(a_{j,\mathbf{k}}^\dagger a_{j,\mathbf{k}}+a_{j,\mathbf{k}}a_{j,\mathbf{k}}^\dagger)$ and effective Hamiltonian $H_{\rm eff}(T)=\int_{L^3}\rho(\mathbf{x})d\mathbf{x}=\sum_{j,\mathbf{k}}\omega_{j,\mathbf{k}}(T)(N_{j,\mathbf{k}}+1/2)$, where the $N_{j,\mathbf{k}}=a_{j,\mathbf{k}}^\dagger a_{j,\mathbf{k}}$ are particle number operators indexed by $j=(n,\Xi)$.

The statistical operator is $\widehat{\rho}=\exp(-H_{\rm eff}(T)/T)$, and the partition function, internal energy and entropy are defined and calculated as stated in Section 2.1. In particular, the total internal energy of lattice vibrations reads $U=\langle H_{\rm eff}\rangle=\sum_j\langle H_{{\rm eff},j}\rangle$,

$$\langle H_{{\rm eff},j}\rangle=\frac{4\pi V}{(2\pi)^3}\int_0^{\Lambda_j(T)}\omega_{j,\mathbf{k}}(T)\left(\frac{1}{e^{\omega_{j,\mathbf{k}}(T)/T}-1}+\frac{1}{2}\right)k^2dk, \tag{6.1}$$

where $U_j=\langle H_{{\rm eff},j}\rangle$ are the partial energies of the atomic oscillators represented by the field component $u_j(\mathbf{x},t)$, $j=(n,\Xi)$. The $\Lambda_j(T)$ are temperature-dependent spectral cutoffs, which can differ for different field components $u_j(\mathbf{x},t)$ (in contrast to monatomic cubic crystals, cf. (2.7)), and the same holds true for the dispersion relations $\omega_{j,\mathbf{k}}=c_{{\rm eff},j}(T)k$ (to be substituted into (6.1)) and the effective phonon speeds $c_{{\rm eff},j}=1/\sqrt{\varepsilon_j(T)\mu_j(T)}$. The averaged effective Hamiltonian of a given atomic species (labeled Ξ in the multi-index $j=(n,\Xi)$) is $\langle H_{{\rm eff},\Xi}\rangle=$

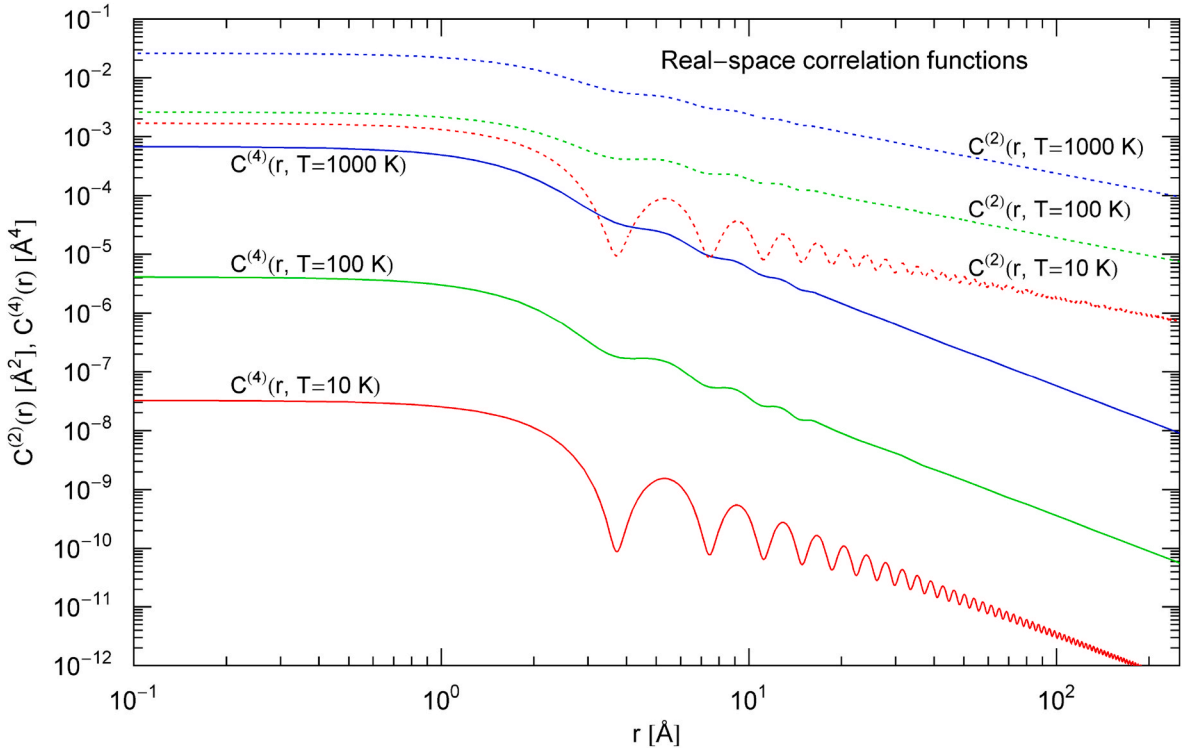

Fig. 7. Effective real-space correlations of lattice vibrations in copper. The two-point correlation $C^{(2)}(r,T)=\langle u_n(\mathbf{x})u_n(\mathbf{y})\rangle_T$ (dotted curves) of the vibrational amplitudes, cf. (2.20) and (3.6), and the reduced four-point function $C^{(4)}(r,T)=\langle(u_n^2(\mathbf{x})-\langle u_n^2(0)\rangle_T)(u_n^2(\mathbf{y})-\langle u_n^2(0)\rangle_T)\rangle_T$ (solid curves) correlating fluctuations around the mean-squared atomic displacement $\langle u_n^2(0)\rangle_T$, cf. (3.2) and (3.3), are assembled with the averages in (5.8) and (5.9). Both correlations are long-range, $C^{(2)}(r,T)=\mathrm{O}(1/r)$ and $C^{(4)}(r,T)=\mathrm{O}(1/r^2)$, and become oscillatory at low temperature, cf. the end of Section 5. At short distance, the correlations are nearly constant and related to the Debye-Waller factors $B(T)$ and $B_2(T)$ in Fig. 6 by $B(T)=8\pi^2C^{(2)}(0,T)$ and $B_2(T)=2\pi^2[2C^{(2)2}(0,T)-C^{(4)}(0,T)]/3$.

$\sum_{n=1}^3\langle H_{\mathrm{eff}\,j=(n,\Xi)}\rangle$. For each atomic species Ξ, anisotropy is modeled by three scalar fields $u_j(\mathbf{x},t)$, $j=(n,\Xi)$, $n=1,2,3$, which are defined by permeability tensors $g_j^{\alpha\beta}$ introduced above.

The partial internal energy density $\widehat{u}_j=\langle H_{\mathrm{eff},j}\rangle/V$ of a field component $u_j(\mathbf{x},t)$ can be written as

$$\widehat{u}_j=\frac{4\pi}{(2\pi)^3}\Lambda_j^3T\left(D(d_j)+\frac{1}{8}d_j\right), \tag{6.2}$$

with $d_j(T)=\theta_j(T)/T$ and Debye temperature $\theta_j(T)=c_{\mathrm{eff},j}(T)\Lambda_j(T)$, and $D(d)$ is the Debye function stated in (2.8). The total internal energy density is $\widehat{u}=\sum_j\widehat{u}_j$. The oscillator density is $n_{\mathrm{oscil}}=\sum_j n_{\mathrm{oscil},j}$, where $n_{\mathrm{oscil},j}=(4\pi/(2\pi)^3)\Lambda_j^3/3$ denotes the partial oscillator density generating the field component $u_j(\mathbf{x},t)$ according to (6.1).

The entropy $S=\sum_j\langle S_j\rangle$ is calculated as in (2.10) and (2.11), where the entropy $\langle S_j\rangle$ of vibrations represented by field component $u_j(\mathbf{x},t)$ reads $\langle S_j\rangle=V\widehat{s}_j$, with partial entropy density

$$\widehat{s}_j=\frac{4\pi}{(2\pi)^3}\Lambda_j^3\left(\frac{4}{3}D(d_j)-\frac{1}{3}\log\left(1-\mathrm{e}^{-d_j}\right)\right), \tag{6.3}$$

so that $\widehat{s}=\sum_j\widehat{s}_j$ is the total entropy density of the lattice vibrations. The basic difference to the thermodynamic functions calculated in Section (2.1) is that both the Debye temperatures $\theta_j(T)$ and the spectral cutoffs $\Lambda_j(T)$ depend on the multi-index $j=(n,\Xi)$ labeling the field components $u_j(\mathbf{x},t)$.

The mean-squared vibrational amplitudes are calculated as in (2.15) and (2.17),

$$\langle u_j^2(T)\rangle=\frac{4\pi}{(2\pi)^3}\frac{\Lambda_j^3T}{\theta_j^2}\frac{1}{\mu_j^{1/2}\varepsilon_j}\left(D_1(d_j)+\frac{1}{4}d_j\right), \tag{6.4}$$

where $\Lambda_j(T)$ is the spectral cutoff of the respective field component, $\theta_j(T)=c_{\mathrm{eff},j}(T)\Lambda_j(T)$ is the Debye temperature, $d_j(T)=\theta_j(T)/T$ a shortcut, and $D_1(d)$ denotes the Debye function in (2.17).

We introduce a temperature-dependent effective oscillator mass $m_{\mathrm{eff},j}(T)$ for each field component and identify the product of the permeabilities in (6.4) as $\mu_j^{1/2}\varepsilon_j=m_{\mathrm{eff},j}n_{\mathrm{oscil},j}$ (cf. (2.18)), where $n_{\mathrm{oscil},j}=(4\pi/(2\pi)^3)\Lambda_j^3/3$ is the oscillator density generating the field component $u_j(\mathbf{x},t)$, $j=(n,\Xi)$, cf. after (6.2). At zero temperature, $m_{\mathrm{eff},j}(T)$ coincides with the atomic mass m_j of the respective atomic species (labeled Ξ in the multi-index $j=(n,\Xi)$). In this way, we can identify the expectation value of the squared field component $\langle u_j^2(T)\rangle$ in (6.4) with the mean-squared vibrational amplitude of normal oscillators belonging to atomic species Ξ and vibrating parallel to the coordinate axis n, cf. (2.19),

$$\langle u_j^2(T)\rangle=\frac{3}{m_{\mathrm{eff},j}(T)}\frac{\hbar^2T}{k_{\mathrm{B}}\theta_j^2(T)}\left(D_1(d_j(T))+\frac{1}{4}d_j(T)\right). \tag{6.5}$$

The corresponding Debye-Waller B-factors are $B_j=8\pi^2\langle u_j^2(T)\rangle$. The $\langle u_j^2(T)\rangle$ can be found by measuring vibrations $\langle u_{k,\Xi}^2\rangle$ of each atomic species Ξ in the formula unit along three independent (but not necessarily mutually orthogonal) diffraction unit vectors $\mathbf{q}_k$ orthogonal to Bragg planes. The coordinate vectors $\langle u_{k,\Xi}^2\rangle\mathbf{q}_k$ define three points on an ellipsoid whose principal axes can be identified with the amplitudes $\langle u_j^2(T)\rangle$ of normal vibrations parallel to the coordinate axes. The $\langle u_j^2(T)\rangle$ in (6.5) can thus be obtained from the measured $\langle u_{k,\Xi}^2\rangle$ by solving a linear system; the latter can be avoided if the diffraction unit vectors $\mathbf{q}_k$ are parallel to the coordinate axes. In the case of cubic lattice symmetry, the ellipsoid degenerates into a sphere.

We write the spectral cutoffs of the lattice internal energy (6.2) and entropy (6.3) as $\Lambda_j(T) = n_{\rm at}^{1/3}h_j(T)$, where $n_{\rm at}$ is the atomic density (atoms per unit volume) of the crystal and $h_j(T)$ are dimensionless scale factors, and convert to molar quantities. Multi-index notation $j = (n,\Xi)$ will be used, where $\Xi = 1,\ldots,N$ labels the atomic species of the compound and $n = 1,2,3$ the corresponding normal vibrations. For monatomic crystals, the index Ξ can be dropped. The molar internal energy and entropy read $U = \sum_j U_j$ and $S = \sum_j S_j$,

$$U_j(T) = \frac{4\pi}{(2\pi)^3}n_{a/m}Rh_j^3T\left(D(d_j)+\frac{d_j}{8}\right),$$
$$S_j(T) = \frac{4\pi}{(2\pi)^3}n_{a/m}Rh_j^3\left[\frac{4}{3}D(d_j)-\frac{1}{3}\log\left(1-\mathrm{e}^{-d_j}\right)\right], \tag{6.6}$$

where $n_{a/m}$ denotes the number of atoms per molecule or formula unit, R is the gas constant and $d_j = \theta_j(T)/T$, cf. Section 4.1. $U_j(T)$ and $S_j(T)$ are the molar internal energy and entropy of phonons represented by the field component $u_j(\mathbf{x},t)$. The total internal energy and entropy are related to the molar lattice heat capacity $C_V(T)$ by $U(T) = \int_0^T C_V(T)\mathrm{d}T + U_0$ and $S(T) = \int_0^T C_V(T)/T\mathrm{d}T$, where the zero-point internal energy U_0 is an integration constant, cf. after (4.2). In Section 6.2, we will calculate U_0 from zero-temperature limits of Debye-Waller factors, and the heat capacity is obtained by least-squares regression as in Section 5.

We specialize the Debye temperatures and spectral cutoffs of each field component $u_j(\mathbf{x},t)$, $j = (n,\Xi)$, as

$$\theta_j(T) = \widehat{c}_j\theta(T),\quad \Lambda_j(T) = \chi_j^{1/3}\Lambda(T), \tag{6.7}$$

where the $\widehat{c}_j$ are positive temperature-independent constants. This ansatz is sufficiently general to model the empirical heat capacity and the Debye-Waller factors of each atomic species of the compound. The multi-index $j = (n,\Xi)$ labels the normal oscillations of the atomic species $\Xi = 1,\ldots,N$ along the coordinate axes $n = 1,2,3$, each atom being represented by three one-dimensional oscillators. The partial density of an atomic species Ξ is $n_{{\rm at},j} = \chi_j n_{\rm at}$, where $\sum_\Xi \chi_{(n,\Xi)} = 1$, with $\chi_{(n,\Xi)} > 0$, and $n_{\rm at}$ is the total atomic density (atoms per unit volume) of the crystal. That is, $n_{{\rm at},j}$, $j = (n,\Xi)$, is the number density of atomic species Ξ. For instance, in the case of alumina Al_2O_3, we have $\Xi = 1,2$ and $\chi_{(n,1)} = 2/5$, $\chi_{(n,2)} = 3/5$. In the case of elemental crystals, $\Xi = 1$, $\chi_{(n,1)} = 1$, so that the index Ξ can be dropped ($j = n = 1,2,3$), and all three field components have the same cutoff $\Lambda_j = \Lambda(T)$, even in the case of anisotropic elemental crystals where only the Debye temperatures $\theta_j(T)$ differ.

In the spectral cutoff in (6.7), we can identify $\chi_j = \chi_\Xi$, since χ_j is independent of the coordinate index n, and note $\sum_j\chi_j = 3$, $j = (n,\Xi)$. We also write $\Lambda(T) = n_{\rm at}^{1/3}h(T)$, with a dimensionless scale factor $h(T)$, so that $\Lambda_j(T) = n_{\rm at}^{1/3}h_j(T)$ with $h_j(T) = \chi_j^{1/3}h(T)$ and define the shortcuts $d_j(T) = \widehat{c}_j d(T)$ and $d(T) = \theta(T)/T$. The effective phonon speed of each field component is defined by $c_{{\rm eff},j}(T) = \theta_j(T)/\Lambda_j(T)$ and $c_{\rm eff}(T) = \theta(T)/\Lambda(T)$, so that $c_{{\rm eff},j}(T) = \widehat{c}_j\chi_j^{-1/3}c_{\rm eff}(T)$ according to (6.7). The oscillator density is $n_{\rm oscil} = \sum_j n_{{\rm oscil},j}$, composed of partial densities $n_{{\rm oscil},j} = (4\pi/(2\pi)^3)\chi_j\Lambda^3/3$, cf. after (6.2), and the series can be summed to $n_{\rm oscil} = (4\pi/(2\pi)^3)\Lambda^3$, with $\Lambda^3 = n_{\rm at}h^3(T)$.

By substituting the Debye temperatures $\theta_j(T) = \widehat{c}_j\theta(T)$ and spectral cutoffs $h_j(T) = \chi_j^{1/3}h(T)$ into the internal energy and entropy (6.6), we find the analog to Eq. (4.3),

$$\frac{3}{4}\frac{TS(T)}{U(T)} = \Delta(d),\quad \Delta(d) := 1-\frac{\sum_j\chi_j\left(2\log\left(1-\mathrm{e}^{-d_j}\right)+d_j\right)}{\sum_j\chi_j\left(8D(d_j)+d_j\right)}, \tag{6.8}$$

with $d_j = \widehat{c}_j d$ and $d(T) = \theta(T)/T$. As in the monatomic isotropic case in (4.3), $\Delta(d)$ is a strictly monotonously decreasing function (from infinity to zero) on the positive real axis, for any choice of positive constants $\widehat{c}_j$ and χ_j, and is, therefore, invertible. It will also be necessary to explicitly invert $\Delta(d)$ in order to calculate $d(T) = \theta(T)/T$ by solving (6.8), $\theta(T) = T\Delta^{-1}((3/4)TS(T)/U(T))$. In Section 6.2, it will be demonstrated that the constants $\widehat{c}_j$ on which the $d_j = \widehat{c}_j d$ in (6.8) depend can be obtained from zero-temperature limits of measured Debye-Waller factors, so that the numerical inversion of $\Delta(d)$ needs to be done only once, with a predetermined set of parameters $\widehat{c}_j$ and χ_j. The constants χ_j are already determined by the atomic composition of the compound, cf. after (6.7).

The cutoff factor $\Lambda(T) = n_{\rm at}^{1/3}h(T)$ in (6.7) is found by solving $U = \sum_j U_j$ in (6.6) (with $h_j(T) = \chi_j^{1/3}h(T)$ and $d_j(T) = \widehat{c}_j\theta(T)/T$ substituted, cf. after (6.7)) for $h(T)$,

$$h(T) = \left(\frac{(2\pi)^3}{4\pi}\frac{U(T)}{n_{a/m}RT\sum_j\chi_j\left(D(d_j)+d_j/8\right)}\right)^{1/3}, \tag{6.9}$$

and the spectral cutoffs of the field components are assembled as $\Lambda_j(T) = n_{\rm at}^{1/3}\chi_j^{1/3}h(T)$, cf. (6.7).

6.2. Zero-point lattice energy of anisotropic compounds

At low temperature, the lattice heat capacity scales as $C_V(T\to 0) \sim c_{V0}T^3$, so that the internal energy converges to its zero-point limit, $U(T\to 0) \sim U_0$, and the lattice entropy scales as $S(T\to 0) \sim c_{V0}T^3/3$, cf. Section 4.3. Accordingly, the left-hand side of Eq. (6.8) reads as stated in (4.9). The asymptotic limit of the right-hand side $\Delta(d)$ of (6.8) reads

$$\Delta(d\to\infty) \sim \frac{8\pi^4}{15}\frac{1}{d^4}\frac{\sum_j\chi_j/\widehat{c}_j^3}{\sum_j\chi_j\widehat{c}_j}, \tag{6.10}$$

where we used $D(d\to\infty) \sim \pi^4/(15d^3)$. Equating this to (4.9) according to (6.8) and solving for d gives the zero-temperature limit of the Debye temperature,

$$\theta_{T=0} = Td(T\to 0) = \left(\frac{32\pi^4}{15}\frac{U_0}{c_{V0}}\frac{\sum_j\chi_j/\widehat{c}_j^3}{\sum_j\chi_j\widehat{c}_j}\right)^{1/4}. \tag{6.11}$$

By substituting the Debye temperatures $\theta_j(T) = \widehat{c}_j\theta(T)$ and spectral cutoffs $h_j(T) = \chi_j^{1/3}h(T)$ defined in (6.7) into the internal energy (6.6) and using the shortcuts $d = \theta(T)/T$ and $d_j(T) = \theta_j(T)/T$, we find

$$U(d\to\infty) \sim \frac{4\pi}{(2\pi)^3}n_{a/m}Rh^3(T)\frac{1}{8}\theta(T)\sum_j\chi_j\widehat{c}_j. \tag{6.12}$$

Equating this limit with the zero-point energy $U(T\to 0) \sim U_0$ and solving for the cutoff factor $h(T)$ gives

$$h_{T=0} = \left(\frac{(2\pi)^3}{4\pi}\frac{8U_0}{n_{a/m}R}\frac{1}{\theta_{T=0}}\frac{1}{\sum_j\chi_j\widehat{c}_j}\right)^{1/3}. \tag{6.13}$$

Analogously, substitution of (6.7) into the mean-squared displacement (6.5) leads to the zero-temperature ($d\to\infty$) limit of the B-factors,

$$B_{j,T=0} = 8\pi^2\frac{3}{m_{{\rm eff},j}(0)}\frac{1}{4}\frac{\hbar^2}{k_{\rm B}\widehat{c}_j\theta_{T=0}}, \tag{6.14}$$

where we used the asymptotic limit of the Debye function stated after (B.4). The zero-temperature limit of the effective oscillator mass is the atomic mass, $m_{{\rm eff},j}(T=0) = m_j$, of the atomic species labeled $\Xi = 1,\ldots,N$ in the multi-index $j = (n,\Xi)$. (At finite temperature, $m_{{\rm eff},j}(T)$ also depends on the coordinate index $n = 1,2,3$. That is, the oscillators generating the normal vibrations have different effective mass, even if they belong to the same atomic species Ξ.)

Eq. (6.14) is a system of $3N$ equations that can be written as

$$b_j = \frac{1}{\widehat{c}_j \theta_{T=0}}, \quad b_j := \frac{1}{6\pi^2}\frac{k_B}{\hbar^2} B_{j,T=0} m_j, \tag{6.15}$$

with multi-index $j = (n, \Xi)$ mapped onto $j = 1,...,3N$. The solution of this system for $\theta_{T=0}$ and $\widehat{c}_j$, $j = 2, ..., 3N$, reads $\theta_{T=0} = 1/(\widehat{c}_1 b_1)$ and $\widehat{c}_j = \widehat{c}_1 b_1/b_j$. We also solve Eq. (6.11) for U_0 and substitute the indicated solution of (6.15), to find the zero-point internal energy

$$U_0 = \frac{15}{32\pi^4} c_{V0} \theta_{T=0}^4 \frac{\sum_j \chi_j \widehat{c}_j}{\sum_j \chi_j/\widehat{c}_j^3} = \frac{15}{32\pi^4} c_{V0} \frac{\sum_j \chi_j/b_j}{\sum_j \chi_j b_j^3}, \tag{6.16}$$

where the b_j are a shortcut for the rescaled zero-temperature limits of the B-factors in (6.15), and c_{V0} is the empirical amplitude of the low-temperature lattice heat capacity, $C_V \sim c_{V0} T^3$. The coefficients χ_j only depend on the formula unit of the compound, see after (6.7).

The constant $\widehat{c}_1$ has dropped out in the second identity in (6.16). In fact, one of the temperature-independent constants $\widehat{c}_j$ introduced in (6.7) can be absorbed into the Debye temperature $\theta(T)$, so that we can put $\widehat{c}_1 = 1$ from the outset, without loss of generality. The constants $\widehat{c}_j$ defining the Debye temperatures $\theta_j = \widehat{c}_j \theta(T)$ of the respective field components $u_j(\mathbf{x}, t), j = (n, \Xi)$, in (6.7) can thus be inferred from the zero-temperature limits $B_{j,T=0}$ of the empirical B-factors and from the mass m_j of the atomic constituents of the compound,

$$\widehat{c}_j = \frac{b_1}{b_j} = \frac{B_{1,T=0} m_1}{B_{j,T=0} m_j}, \tag{6.17}$$

indexed by $j = 1, ..., 3N$, cf. after (6.15).

In Eq. (6.16), we substitute the shortcut b_j defined in (6.15), to find

$$U_0 = \frac{15}{32\pi^4} \left(\frac{\hbar^2}{k_B} 6\pi^2\right)^4 c_{V0} \frac{\sum_j \chi_j / \left(B_{j,T=0} m_j\right)}{\sum_j \chi_j \left(B_{j,T=0} m_j\right)^3}, \tag{6.18}$$

where the summations are over the multi-index $j = (n, \Xi)$. In this way, the zero-point energy U_0 can be calculated from the zero-temperature limits of the B-factors and the amplitude c_{V0} of the low-temperature lattice heat capacity. In the case of elemental cubic crystals, Eq. (6.18) simplifies to (4.14).

We can now proceed as in Section 5 for copper. First, we use a multiply broken power law as in (5.1) to regress the heat capacity from empirical data. With this analytic fit, we can obtain the thermal component of the internal energy $U(T) = \int_0^T C_V(T) \mathrm{d}T + U_0$ and entropy $S(T) = \int_0^T C_V(T)/T \mathrm{d}T$, as indicated after (6.6). The amplitude c_{V0} of the low-temperature heat capacity can also be extracted from the least-squares fit of the heat capacity as done in Section 5.1 for copper. The zero-point lattice energy U_0 is calculated by way of (6.18), using c_{V0}, the zero-temperature limits of the empirical Debye-Waller factors $B_{j,T=0}$, the atomic masses m_j and the factors χ_j which can be read off from the formula unit, cf. after (6.7).

The constants $\widehat{c}_j$ defining the Debye temperatures $\theta_j(T) = \widehat{c}_j \theta(T)$ of the field components in (6.7) are calculated from the empirical zero-temperature limits $B_{j,T=0}$ and the atomic masses m_j by way of (6.17). The constants $\widehat{c}_j$ and χ_j completely determine the function $\Delta(d)$ in (6.8). After numerical inversion of $\Delta(d)$, the Debye temperature $\theta(T)$ in (6.7) is found via $\theta(T) = T\Delta^{-1}((3/4)TS(T)/U(T))$, see after (6.8). Subsequently, the cutoff factors $\Lambda_j(T) = \chi_j^{1/3} \Lambda(T)$ of the field components in (6.7) are calculated via (6.9). The Debye temperatures $\theta_j(T)$ and cutoff factors $\Lambda_j(T)$ determine the temperature evolution of the partial internal energies (6.2) and entropies (6.3) of the field components. The effective temperature-dependent oscillator masses $m_{\mathrm{eff},j}(T)$ are calculated by way of (6.5), where we substitute the empirical temperature evolution of the mean-squared vibrations $\langle u_j^2(T)\rangle = B_j(T)/(8\pi^2)$.

7. Conclusion

The effective field theory of phonons developed here can accurately model thermodynamic variables and Debye-Waller factors of lattice vibrations and is applicable to elemental cubic crystals as well as anisotropic compounds. The formalism is based on a multi-component scalar field whose components $u_j(\mathbf{x}, t)$ are generated by the normal vibrations of the atomic constituents, cf. Section 6. The internal energy and entropy of each field component is determined by a temperature-dependent spectral cutoff $\Lambda_j(T)$ and Debye temperature $\theta_j(T)$. The Debye temperatures and spectral cutoffs of different field components differ in general, the exception being monatomic cubic crystals where the field components admit the same spectral cutoff $\Lambda(T)$ and Debye temperature $\theta(T)$, cf. Section 2.1 and the beginning of Section 3.

The varying Debye temperatures and spectral cutoffs are extracted from the experimental lattice heat capacity and low-temperature Debye-Waller B-factors, as explained in Sections 4 and 6 and illustrated with the copper lattice in Section 5. The effective phonon speed $c_{\mathrm{eff},j}(T)$ defining the dispersion relation and partial oscillator density of each field component $u_j(\mathbf{x}, t)$ can be determined from the Debye temperatures $\theta_j(T)$ and spectral cutoffs $\Lambda_j(T)$. The effective oscillator mass $m_{\mathrm{eff},j}(T)$ of the normal vibrations generating the field component $u_j(\mathbf{x}, t)$ enters as normalization factor in the quantized $u_j(\mathbf{x}, t)$ and can be calculated from the empirical temperature evolution of the corresponding $B_j(T)$ factor, cf. Sections 5 and 6.2. The oscillator mass does not affect the entropy and internal energy of the vibrations, as it drops out in the partition function.

The proposed phenomenological field theory is non-perturbative, avoiding the use of anharmonic additions to the oscillator potential [42,43], and does not require band structure calculations, as it is based on a uniform density of states like the Debye theory. Anharmonicity is dealt with effectively, by coupling the field components to temperature-dependent permeability tensors resulting in temperature-dependent dispersion relations, cf. Sections 2.1 and 6.1.

An often employed method to model the empirical lattice heat capacity is to use the Debye theory with constant Debye temperature and spectral cutoff and add Einstein terms at measured optical frequencies. Once the Einstein and Debye temperatures are fixed, there is only one free fitting parameter left determining the overall contribution of the Einstein terms, so that an accurate fit of the heat capacity over the full temperature range of the solid phase is unlikely to be achieved in this way, not to mention the modeling of the empirical temperature evolution of the B-factors from diffraction data, which regularly indicate larger B-factors at high temperatures close to the melting point than predicted by the Debye theory with constant Debye temperature.

In contrast to the Debye theory, where the zero-point energy of the phonons is already determined by the constant Debye temperature, cf. Section 5, the zero-point internal energy U_0 emerges as integration constant in the temperature-dependent spectral cutoffs $\Lambda_j(T)$ and Debye temperatures $\theta_j(T)$, cf. Sections 4.1 and 6.1. The Debye-Waller factors $B_j(T)$ also depend on U_0 by way of the Debye temperatures $\theta_j(T)$, especially in the low-temperature regime, cf. Section 4.2 and 6.2. Therefore, the zero-point internal energy can be estimated from the zero-temperature limits of the measured B-factors, as done in Section 5 for copper.

The high- and low-temperature limits of the lattice heat capacity coincide with those of the standard Debye model, cf. Section 5, whereas the intermediate temperature range of the experimental heat capacity can more accurately be reproduced by the varying $\theta_j(T)$ and $\Lambda_j(T)$. This is exemplified with copper in Fig. 1, where an inflection point arises in the double-logarithmic plot of the empirical lattice heat capacity, unaccounted for by the Debye theory. The empirical temperature dependence of the Debye-Waller B-factor of copper can also be modeled more accurately with a varying Debye temperature and oscillator mass, especially at high temperature where the observed slope of $B(T)$ in log-log plots is noticeably steeper than the linear temperature scaling of the

Debye model, cf. Section 5 and Fig. 6. In contrast to the Debye theory, there is no practical need to distinguish between caloric and X-ray Debye temperatures, as the Debye temperatures $\theta_j(T)$ extracted from the empirical heat capacity are identical to those used in the modeling of the Debye-Waller B-factors.

Effective correlation functions of lattice vibrations of elemental cubic crystals were calculated in Sections 2.2, 3 and 5. Since this effective field theory is non-perturbative, deviations from harmonicity being modeled by permeability tensors rather than by anharmonic interaction terms added to the quadratic oscillator potential, it was possible to derive closed integral representations of the spatial correlations, which depend on the empirically inferred functions $\theta(T)$, $\Lambda(T)$ and $m_{\rm eff}(T)$. The effective two-point correlation function of elemental cubic crystals was calculated in Section 2.2, the reduced four-point correlation of fluctuations around the mean-squared atomic displacement in Section 3, and the long-distance asymptotics of the correlations in Appendix A. The second-order Debye-Waller factor $B_2(T)$ emerging in the cumulant expansion of the Debye-Waller intensity factor $\exp(-2M)$ was assembled from the short-distance limits of the two-point and four-point correlations, cf. Section 3 and 5, and is plotted for copper in Fig. 6. The correlation functions of the copper lattice are depicted in Fig. 7. The correlations are long-range with power-law decay above 10 Å and nearly constant at short distance ≤ 1 Å. At low temperature, oscillations emerge in the crossover region, which become attenuated in the power-law tails.

Declaration of competing interest

The author declares that he has no known competing financial interests or personal relationships that could have appeared to influence the work reported in this paper.

Appendix A. Derivation of the equal-time four-point correlation of lattice vibrations and its long-range asymptotics

By making use of the commutation relation $[a_{j,\mathbf{k}}, a^\dagger_{l,\mathbf{k}'}] = \delta_{\mathbf{k}\mathbf{k}'}\delta_{jl}$ and the Fourier decomposition of the field component u_n in (3.1), the squared u_n^2 can be written as

$$u_n^2(\mathbf{x}) = \frac{1}{L^3}\sum_{\mathbf{k}\neq\mathbf{k}'}\frac{1}{\sqrt{\mu^{1/2}\varepsilon\omega_{\mathbf{k}}}}\frac{1}{\sqrt{\mu^{1/2}\varepsilon\omega_{\mathbf{k}'}}}a^\dagger_{n,\mathbf{k}}a_{n,\mathbf{k}'}\,\mathrm{e}^{\mathrm{i}(\mathbf{k}-\mathbf{k}')\mathbf{x}} + u_n^2(0),$$
$$u_n^2(0) = \frac{1}{L^3}\sum_{\mathbf{k}}\frac{1}{\mu^{1/2}\varepsilon\omega_{\mathbf{k}}}\left(N_{n,\mathbf{k}}+\frac{1}{2}\right). \tag{A.1}$$

This applies when restricted to expectation values, and the time-dependent exponentials have been dropped, as they do not affect the subsequent equal-time averages. We substitute this expansion into the correlation average $C^{(4)}(\mathbf{x},\mathbf{y};T)$ in (3.2) and use the identity, cf. Ref. [30],

$$\sum_{m\neq n,k\neq l}a^\dagger_m a_n a^\dagger_k a_l = \sum_{k\neq k'}N_k(1+N_{k'}) \tag{A.2}$$

(in multi-index notation, with particle number operators $N_i = a_i^\dagger a_i$, $i=(n,\mathbf{k})$ and fixed n, cf. after (2.5)), to obtain

$$C^{(4)}(\mathbf{x},\mathbf{y};T) = \left\langle\frac{1}{L^6}\sum_{\mathbf{k}\neq\mathbf{k}}\frac{1}{\mu^{1/2}\varepsilon\omega_{\mathbf{k}}}\frac{1}{\mu^{1/2}\varepsilon\omega_{\mathbf{k}'}}N_{n,\mathbf{k}}\left(1+N_{n,\mathbf{k}'}\right)\mathrm{e}^{\mathrm{i}(\mathbf{k}-\mathbf{k}')(\mathbf{x}-\mathbf{y})}\right\rangle_T. \tag{A.3}$$

This average can be simplified by applying the factorization identity

$$\left\langle\frac{1}{L^6}\sum_{k,k'}c_k d_{k'}N_kN_{k'}\right\rangle_T = \left\langle\frac{1}{L^3}\sum_k c_kN_k\right\rangle_T\left\langle\frac{1}{L^3}\sum_{k'}d_{k'}N_{k'}\right\rangle_T, \tag{A.4}$$

valid in the thermodynamic limit [29]; the coefficients c_k and $d_{k'}$ in (A.4) can be arbitrarily chosen. (The restriction $\mathbf{k}\neq\mathbf{k}'$ in summation (A.4) can also be lifted in the continuum limit $L\to\infty$.) In this way, we find the reduced four-point function (3.2) as $C^{(4)}(\mathbf{x},\mathbf{y};T) = \langle\widehat{A}\rangle_T^2 + \langle\widehat{B}\rangle_T\langle\widehat{A}\rangle_T$, where $\widehat{A}(\mathbf{x},\mathbf{y})$ and $\widehat{B}(\mathbf{x},\mathbf{y})$ denote the operators

$$\widehat{A} = \frac{1}{L^3}\sum_{\mathbf{k}}\frac{\mathrm{e}^{\mathrm{i}\mathbf{k}(\mathbf{x}-\mathbf{y})}}{\mu^{1/2}\varepsilon\omega_{\mathbf{k}}}N_{n,\mathbf{k}},\quad \widehat{B} = \frac{1}{L^3}\sum_{\mathbf{k}}\frac{\mathrm{e}^{\mathrm{i}\mathbf{k}(\mathbf{x}-\mathbf{y})}}{\mu^{1/2}\varepsilon\omega_{\mathbf{k}}}, \tag{A.5}$$

which admit the finite-temperature expectation values, cf. (2.6),

$$\left\langle\widehat{A}(\mathbf{x},\mathbf{y})\right\rangle_T = \frac{1}{(2\pi)^3}\int_0^{\Lambda(T)}\frac{\mathrm{e}^{\mathrm{i}\mathbf{k}(\mathbf{x}-\mathbf{y})}}{\mu^{1/2}\varepsilon\omega_{\mathbf{k}}}\frac{k^2\mathrm{d}k\mathrm{d}\Omega_{\mathbf{k}_0}}{\mathrm{e}^{\omega_{\mathbf{k}}/T}-1}, \tag{A.6}$$

$$\left\langle\widehat{B}(\mathbf{x},\mathbf{y})\right\rangle_T = \frac{1}{(2\pi)^3}\int_0^{\Lambda(T)}\frac{\mathrm{e}^{\mathrm{i}\mathbf{k}(\mathbf{x}-\mathbf{y})}}{\mu^{1/2}\varepsilon\omega_{\mathbf{k}}}k^2\mathrm{d}k\mathrm{d}\Omega_{\mathbf{k}_0}. \tag{A.7}$$

Here, $\mathrm{d}\Omega_{\mathbf{k}_0}$ indicates integration over the solid angle, leading to the averages $\langle\widehat{A}(r)\rangle_T$ and $\langle\widehat{B}(r)\rangle_T$ defining the correlation $C^{(4)}(r,T)=C^{(4)}(\mathbf{x},\mathbf{y};T)$ stated in (3.3)-(3.5).

We briefly discuss the long-range asymptotics of the four-point correlation $C^{(4)}(r,T)$ defined in (3.3) as well as the asymptotics of the expectation values (3.6) and (3.8), which only depend on the averages $\langle\widehat{A}(r)\rangle_T$ and $\langle\widehat{B}(r)\rangle_T$ stated in (3.4) and (3.5), and $\langle\widehat{B}(r)\rangle_T$ is elementary.

The long-distance asymptotics of $\langle\widehat{A}(r)\rangle_T$ in (3.4) is obtained from the integral, cf. Ref. [32],

$$\int_0^\infty \frac{\sin(kr)}{kr}\frac{k\mathrm{d}k}{\mathrm{e}^{c_{\mathrm{eff}}k/T}-1}=\frac{1}{r}\frac{\pi}{2}\frac{T}{c_{\mathrm{eff}}}-\frac{1}{2r^2}+\frac{1}{r}\frac{\pi}{2}\frac{T}{c_{\mathrm{eff}}}\frac{2}{\mathrm{e}^{2\pi rT/c_{\mathrm{eff}}}-1}, \tag{A.8}$$

by subtraction of the leading-order Fourier asymptotics

$$\int_\Lambda^\infty \frac{\sin(kr)}{kr}\frac{k\mathrm{d}k}{\mathrm{e}^{c_{\mathrm{eff}}k/T}-1}\sim\frac{\cos(\Lambda r)}{r^2}\frac{1}{\mathrm{e}^{c_{\mathrm{eff}}\Lambda/T}-1}+\mathrm{O}\big(1/r^3\big), \tag{A.9}$$

so that

$$\big\langle\widehat{A}(r)\big\rangle_T=\frac{4\pi}{(2\pi)^3}\frac{1}{\mu^{1/2}\varepsilon c_{\mathrm{eff}}}\frac{\pi T}{2c_{\mathrm{eff}}r}\left[1-\frac{c_{\mathrm{eff}}}{\pi Tr}\left(1+\frac{2\cos(\Lambda r)}{\mathrm{e}^{c_{\mathrm{eff}}\Lambda/T}-1}\right)+\mathrm{O}\big(1/r^2\big)\right]. \tag{A.10}$$

Here, we substitute $c_{\mathrm{eff}}=\theta(T)/\Lambda(T)$, cf. after (2.8), and $\mu^{1/2}\varepsilon=4\pi m_{\mathrm{eff}}(T)\Lambda^3(T)/\big(3(2\pi)^3\big)$, cf. (2.18), and restore the units to obtain

$$\big\langle\widehat{A}(r)\big\rangle_T=\frac{3}{m_{\mathrm{eff}}}\frac{\hbar^2T}{k_{\mathrm{B}}\theta^2}\frac{\pi}{2\Lambda r}\left[1-\frac{\theta}{\pi T\Lambda r}\left(1+\frac{2\cos(\Lambda r)}{\mathrm{e}^{\theta/T}-1}\right)+\mathrm{O}\big(1/r^2\big)\right], \tag{A.11}$$

which is the asymptotic expansion of $\langle\widehat{A}(r)\rangle_T$ in (3.11). This expansion is applicable as long as the temperature-dependent second-order term in the brackets stays much smaller than one.

The long-range asymptotics of the two-point correlation $C^{(2)}(r,T)=\langle u_n(\mathbf{x})u_n(\mathbf{y})\rangle_T$ in (3.6) is also defined by (A.11) and $\langle\widehat{B}(r)\rangle_T$ in (3.12), and the same holds true for the unreduced four-point function (3.8), with $\langle\widehat{A}(0)\rangle_T$ and $\langle\widehat{B}(0)\rangle_T$ in (3.11) and (3.12). In leading order, $\langle\widehat{A}(r)\rangle_T\propto 1/\,r$ (non-oscillatory) and $\langle\widehat{B}(r)\rangle_T=\mathrm{O}(1/r^2)$. The constant leading orders of the correlations in the opposite short-distance regime are determined by the finite limit values $\langle\widehat{A}(r=0)\rangle_T$ and $\langle\widehat{B}(r=0)\rangle_T$ in (3.11) and (3.12).

Appendix B. $\theta(T)/T\to 0,\infty$ asymptotics of thermodynamic variables

We use the shortcut $d=\theta(T)/T$ for the expansion parameter. In Sections 4.2 and 4.3, we need the subsequent asymptotic limits to demonstrate that both $\theta(T\to 0)$ and $\theta(T\to\infty)$ converge to finite limit values and to calculate these limits. The $d\to 0,\infty$ limits of the molar internal energy (4.1) and entropy (4.2) read

$$U_{d\to 0}\sim\frac{4\pi}{(2\pi)^3}n_{a/m}Rh^3T,\quad U_{d\to\infty}\sim\frac{4\pi}{(2\pi)^3}n_{a/m}Rh^3\frac{3\theta}{8}, \tag{B.1}$$

and

$$S_{d\to\infty}\sim\frac{4\pi}{(2\pi)^3}n_{a/m}Rh^3\frac{4\pi^4}{15}\frac{1}{d^3},\ S_{d\to 0}\sim\frac{4\pi}{(2\pi)^3}n_{a/m}Rh^3\left(-\log d+\frac{4}{3}\right). \tag{B.2}$$

The $d\to 0,\infty$ limits of the monotonously decreasing function $\Delta(d)$ in (4.3) are

$$\Delta(d\to\infty)\sim\frac{8\pi^4}{15}\frac{1}{d^4},\quad \Delta(d\to 0)\sim-\frac{3}{4}\log d+1. \tag{B.3}$$

Eqs. (B.1)-(B.3) can be derived from the respective limits of the Debye function in (2.8), $D(d\to 0)\sim 1/3$ and $D(d\to\infty)\sim\pi^4/(15d^3)$.

The $d\to 0,\infty$ asymptotics of the mean-squared vibrations $\langle u_n^2(0)\rangle_T$ in (2.19) reads

$$\big\langle u_n^2(0)\big\rangle_{T,d\to 0}\sim\frac{3}{m_{\mathrm{eff}}}\frac{\hbar^2T}{k_{\mathrm{B}}\theta^2},\quad \langle u_n^2(0)\rangle_{T,d\to\infty}\sim\frac{3}{4}\frac{1}{m_{\mathrm{eff}}}\frac{\hbar^2}{k_{\mathrm{B}}\theta}, \tag{B.4}$$

where we used the limits $D_1(d\to 0)\sim 1$ and $D_1(d\to\infty)\sim\pi^2/(6d)$ of the Debye function in (2.17). The $d\to 0,\infty$ limits of the cumulant $\widehat{\kappa}_T=3\langle u_n^2(0)\rangle_T^2-\langle u_n^4(0)\rangle_T$ in (4.6) are

$$\widehat{\kappa}_{T,d\to 0} \sim \left(\frac{3}{m_{\rm eff}}\frac{\hbar^2 T}{k_{\rm B}\theta^2}\right)^2,\ \widehat{\kappa}_{T,d\to\infty} \sim \frac{1}{8}\left(\frac{3}{m_{\rm eff}}\frac{\hbar^2}{k_{\rm B}\theta}\right)^2, \tag{B.5}$$

which are related to the respective limits of the mean-squared vibrations (B.4) by $\widehat{\kappa}_{T,d\to 0} \sim \langle u_n^2(0)\rangle^2_{T,d\to 0}$ and $\widehat{\kappa}_{T,d\to\infty} \sim 2\langle u_n^2(0)\rangle^2_{T,d\to\infty}$.

References

[1] W. Tian, J. Cai, H. Chen, J. Phys. Chem. Solid. 106 (2017) 10.
[2] S. Yousuf, D.C. Gupta, J. Phys. Chem. Solid. 108 (2017) 109.
[3] J.H. Tian, T. Song, X.W. Sun, T. Wang, G. Jiang, J. Phys. Chem. Solid. 110 (2017) 70.
[4] X.-W. Sun, Z.-J. Liu, W.-L. Quan, T. Song, R. Khenata, S. Bin-Omran, J. Phys. Chem. Solid. 116 (2018) 209.
[5] B. Adivaiah, E.N. Rao, T.A. Parveen, G. Vaitheeswaran, J. Phys. Chem. Solid. 122 (2018) 268.
[6] C. Liu, M. Chen, J. Li, L. Liu, P. Li, M. Ma, C. Shao, J. He, T. Liang, J. Phys. Chem. Solid. 130 (2019) 58.
[7] Y. Zhong, H. Mei, D. He, X. Du, N. Cheng, J. Phys. Chem. Solid. 134 (2019) 157.
[8] S.A. Khandy, D.C. Gupta, J. Phys. Chem. Solid. 135 (2019) 109079.
[9] R. Tomaschitz, Physica B 593 (2020) 412243.
[10] S.A. Sofi, D.C. Gupta, Int. J. Quant. Chem. 120 (2020), e26216.
[11] T.M. Bhat, D.C. Gupta, J. Phys. Chem. Solid. 112 (2018) 190.
[12] S.A. Sofi, D.C. Gupta, Comput. Condens. Matter 19 (2019), e00375.
[13] T.M. Bhat, D.C. Gupta, J. Phys. Chem. Solid. 119 (2018) 281.
[14] S.A. Sofi, D.C. Gupta, Physica B 577 (2020) 411792.
[15] M. Narimani, Z. Nourbakhsh, J. Phys. Chem. Solid. 102 (2017) 121.
[16] S.A. Sofi, D.C. Gupta, Int. J. Energy Res. 44 (2020) 2137.
[17] S.A. Sofi, D.C. Gupta, J. Solid State Chem. 284 (2020) 121178.
[18] Q. Mahmood, N.A. Noor, M. Rashid, B. Ul Haq, A. Laref, I. Qasim, J. Phys. Chem. Solid. 132 (2019) 68.
[19] Q. Zhang, J. Ding, M. He, J. Phys. Chem. Solid. 108 (2017) 76.
[20] E. Jain, G. Pagare, S. Dubey, R. Sharma, Y. Sharma, J. Phys. Chem. Solid. 122 (2018) 246.
[21] Y. Asadi, Z. Nourbakhsh, J. Phys. Chem. Solid. 132 (2019) 213.
[22] R. Moussa, A. Abdiche, R. Khenata, X.T. Wang, D. Varshney, X.W. Sun, S. Bin Omran, A. Bouhemadou, D.P. Rai, J. Phys. Chem. Solid. 119 (2018) 36.
[23] A. Gupta, S.K. Verma, A. Kumari, B.D. Indu, J. Phys. Chem. Solid. 134 (2019) 83.
[24] S. Nandi, Y.M. Jana, H.C. Gupta, J. Phys. Chem. Solid. 115 (2018) 347.
[25] D.S. Tsvetkov, A.L. Sednev-Lugovets, D.A. Malyshkin, V.V. Sereda, A.Yu. Zuev, I. L. Ivanov, J. Phys. Chem. Solid. 147 (2020) 109613.
[26] R. Yang, C. Zhu, Q. Wei, Z. Du, J. Phys. Chem. Solid. 98 (2016) 10.
[27] S. Wang, Y. Zhao, S. Deng, W. Yang, D. Lian, H. Hou, J. Phys. Chem. Solid. 125 (2019) 115.
[28] Y.F. Li, B. Xiao, L. Sun, Y.M. Gao, S.Q. Ma, D.W. Yi, J. Phys. Chem. Solid. 103 (2017) 49.
[29] R. Tomaschitz, Physica A 524 (2019) 130.
[30] L.D. Landau, E.M. Lifshitz, Statistical Physics, third ed., Pergamon, Oxford, 1980.
[31] J.T. Day, J.G. Mullen, R.C. Shukla, Phys. Rev. B 52 (1995) 168.
[32] I.S. Gradshteyn, I.M. Ryzhik, Table of Integrals, Series, and Products, eighth ed., Academic Press, Waltham, Mass., 2015.
[33] G.K. White, M.L. Minges, Int. J. Thermophys. 18 (1997) 1269.
[34] R. Tomaschitz, Physica A 483 (2017) 438.
[35] R. Tomaschitz, Physica A 541 (2020) 123188.
[36] R. Tomaschitz, Appl. Phys. A 126 (2020) 102.
[37] C.K. Shepard, J.G. Mullen, G. Schupp, Phys. Rev. B 61 (2000) 8622.
[38] C.J. Martin, D.A. O'Connor, Acta Crystallogr. A 34 (1978) 500.
[39] C.K. Shepard, J.G. Mullen, G. Schupp, Phys. Rev. B 57 (1998) 889.
[40] C.J. Martin, D.A. O'Connor, J. Phys. C Solid State Phys. 10 (1977) 3521.
[41] T.H.K. Barron, A.J. Leadbetter, J.A. Morrison, L.S. Salter, Acta Crystallogr. 20 (1966) 125.
[42] S.S. Batsanov, J. Phys. Chem. Solid. 144 (2020) 109508.
[43] S.Sh. Rekhviashvili, Kh.L. Kunizhev, High Temp. 55 (2017) 312.